THE JOURNAL OF BIOLOGICAL CHEMISTRY VOL. 287, NO. 8, pp. 5340–5356, February 17, 2012

Toxin-Antitoxin Systems of *Mycobacterium smegmatis* Are Essential for Cell Survival*[S]

Received for publication, July 27, 2011, and in revised form, December 7, 2011 Published, JBC Papers in Press, December 23, 2011, DOI 10.1074/jbc.M111.286856

Rebekah Frampton[‡1], **Raphael B. M. Aggio**[§], **Silas G. Villas-Bôas**[§], **Vickery L. Arcus**[¶], **and Gregory M. Cook**[‡2]

From the [‡]*Department of Microbiology and Immunology, Otago School of Medical Sciences, University of Otago, Dunedin 9054, the* [§]*School of Biological Sciences, University of Auckland, Auckland 1142, and the* [¶]*Department of Biological Sciences, University of Waikato, Private Bag 3105, Hamilton 3240, New Zealand*

Background: Mycobacteria harbor a vast array of toxin-antitoxin modules, but their roles remain largely unknown.
Results: Deletion of all TA modules in *Mycobacterium smegmatis* caused a survival defect and alterations in amino acid metabolism.
Conclusion: We demonstrate an essential role for TA modules in mycobacterial metabolism and survival.
Significance: These results may explain the basis for 88 TA modules in *M. tuberculosis* where metabolism must be tightly controlled.

The role of chromosomal toxin-antitoxin (TA) modules in bacterial physiology remains enigmatic despite their abundance in the genomes of many bacteria. *Mycobacterium smegmatis* contains three putative TA systems, VapBC, MazEF, and Phd/Doc, and previous work from our group has shown VapBC to be a *bona fide* TA system. In this study, we show that MazEF and Phd/Doc are also TA systems that are constitutively expressed, transcribed as leaderless transcripts, and subject to autoregulation, and expression of the toxin component leads to growth inhibition that can be rescued by the cognate antitoxin. No phenotype was identified for deletions of the individual TA systems, but a triple deletion strain (Δ*vapBC, mazEF, phd/doc*), designated ΔTA^{triple}, exhibited a survival defect in complex growth medium demonstrating an essential role for these TA modules in mycobacterial survival. Transcriptomic analysis revealed no significant differences in gene expression between wild type and the ΔTA^{triple} mutant under these conditions suggesting that the growth defect was not at a transcriptional level. Metabolomic analysis demonstrated that in response to starvation in complex medium, both the wild type and ΔTA^{triple} mutant consumed a wide range of amino acids from the external milieu. Analysis of intracellular metabolites revealed a significant difference in the levels of branched-chain amino acids between the wild type and ΔTA^{triple} mutant, which are proposed to play essential roles in monitoring the nutritional supply and physiological state of the cell and linking catabolic with anabolic reactions. Disruption of this balance in the ΔTA^{triple} mutant may explain the survival defect in complex growth medium.

Toxin-antitoxin (TA)[3] systems were first discovered as plasmid stability systems that rely on the constant production of the labile antitoxin to prevent the release of active toxin from the benign protein complex that is normally found in the cell (1, 2). Active toxin may cause cell death to prevent loss of the plasmid within the population, or it may inhibit cell growth to allow the levels of the plasmid to return to normal. TA systems have also been found in bacterial chromosomes, and at present there has been considerable debate about the role of these systems in cell physiology with several hypotheses being presented (3). There are three types of TA systems, and they differ primarily in the interactions between the toxin and the antitoxin to form the benign complex. In type I TA systems, such as the Hok/Sok system of plasmid R1, the antitoxin is a small RNA that inhibits the mRNA of the toxin. The complex in type II systems is composed of two proteins, and the toxic protein of the type III system is inhibited by the antitoxic RNA (4).

Nine families of toxins have been characterized for the type II TA systems (5, 6). Of these, the *mazEF*, *relBE*, and *vapBC* families have been studied in detail. All three of these toxins cleave mRNA; RelE requires the ribosome for RNA cleavage, whereas MazF, HigB, and VapC do not (7–10). The CcdB and ParE toxins inhibit chromosome replication through DNA gyrase (11–13); the Doc toxin inhibits the 30 S subunit of the ribosome (14), and HipA phosphorylates the translation factor EF-Tu (15). Even though the toxins target important components of the cell, the role of chromosomally encoded TA systems has been difficult to determine as the phenotypes appear to be pleiotropic. A five TA deletion strain has been created in *Escherichia coli* where the *mazEF*, *relBE*, *yefM-yoeB*, *chpB,* and *dinJ-yafQ* TA systems have been deleted (16). No phenotypic difference was found in response to stress and recovery responses. However, when Kim *et al.* (17) investigated the role of TA systems in

* This work was supported in part by the Health Research Council New Zealand.
[S] This article contains supplemental Tables S1–S4 and Figs. S1 and S2.
[1] Supported by Ph.D. scholarships from the University of Otago.
[2] To whom correspondence should be addressed: Dept. of Microbiology and Immunology, Otago School of Medical Sciences, University of Otago, P. O. Box 56, Dunedin 9054, New Zealand. Tel.: 64-3-4797722; Fax: 64-3-4798540; E-mail: gregory.cook@otago.ac.nz.

[3] The abbreviations used are: TA, toxin-antitoxin; HdB, Hartmans de Bont medium; MU, Miller units; qPCR, quantitative real time PCR; TPP^+, methyltriphenylphosphonium iodide; TSS, transcriptional start site; ADC, albumin/glucose/catalase enrichment; F, forward; R, reverse; Tc, tetracycline; TSS, transcriptional start site; RACE, rapid amplification of cDNA ends; Doc, death-on-curing protein.

biofilms, they found that this five TA deletion strain had reduced initial biofilm formation and reduced biofilm dispersal. Each of the five TA systems was found to play a different role in the process of forming biofilms, with MazF appearing to be the main effector in the network (18).

Several studies have been performed to identify TA systems in the chromosomes of sequenced bacteria and archaea (19, 20). These findings suggest a large amount of diversity in the number of TA systems in each genome. One group that is of interest is the genus *Mycobacterium*. The number of TA systems in the genome of *Mycobacterium tuberculosis* has been greatly expanded with 88 putative TA systems present (19, 21). In contrast, the chromosome of *Mycobacterium leprae* contains only toxin pseudogenes, whereas *Mycobacterium smegmatis* contains only three TA systems (19, 22). The greatest number of TA modules in *M. tuberculosis* belongs to VapBC with 47 in total. The *vapBC* family of TA systems consists of the antitoxin VapB and the toxin VapC, which is proposed to be an RNase. This family has recently been reviewed (23). There are examples where VapBC systems have been shown to play a role in the adaptation of the bacteria to an environmental niche (*e.g.* epithelial cells and root nodules) (24).

To provide a molecular model for understanding the role of TA systems in mycobacteria, we have characterized all three TA systems in *M. smegmatis* at a molecular level. We show that all three TA systems are *bona fide* TA modules, and deleting all three (*vapBC-mazEF-phd/doc*) in *M. smegmatis* leads to a survival defect in complex growth medium.

EXPERIMENTAL PROCEDURES

Bacterial Strains and Growth Conditions—All strains and plasmids used in this study are listed in Table 1. *E. coli* strains were grown in Luria-Bertani (LB) medium at 37 °C with agitation (200 rpm). *M. smegmatis* strain mc^{2}155 and derived strains were routinely grown at 37 °C, 200 rpm in LB containing 0.05% (w/v) Tween 80 (LBT), in Middlebrook 7H9 medium (Difco) supplemented with 10% albumin/glucose/catalase enrichment (ADC; BD Biosciences) and 0.05% (w/v) Tween 80, or in modified Hartmans de Bont medium (HdB) (25). The composition of this medium per liter was as follows: 10 ml of trace metals, 27.4 mM glycerol, 15 mM ammonium sulfate, 21 mM Na_2HPO_4, and 11 mM KH_2PO_4 and 0.05% Tween 80. For nutrient limitation studies, glycerol was reduced to 11 mM for carbon limitation, ammonium sulfate reduced 100-fold for nitrogen limitation, and Na_2HPO_4 and K_2HPO_4 reduced 100-fold for phosphate limitation. During phosphate limitation, the buffering capacity of the medium was increased by the addition of 50 mM MOPS.

M. smegmatis transformants were grown at 28 °C for propagation of temperature-sensitive vectors and at 40 °C for allelic exchange mutagenesis. Selective media contained kanamycin (50 μg ml^{-1} for *E. coli*; 20 μg ml^{-1} for *M. smegmatis*), gentamicin (20 μg ml^{-1} for *E. coli*; 5 μg ml^{-1} for *M. smegmatis*), hygromycin B (200 μg ml^{-1} for *E. coli*; 50 μg ml^{-1} for *M. smegmatis*), spectinomycin (50 μg ml^{-1} for *E. coli*), streptomycin (50 μg ml^{-1} for *E. coli*, 20 μg ml^{-1} for *M. smegmatis*), and ampicillin (100 μg ml^{-1} for *E. coli*). Solid media contained 1.5% agar.

Growth curves were performed in triplicate in LBT and HdB. Bacterial cell viability was monitored by cell counts based on cfu ml^{-1} where serial dilutions of bacterial cell culture in phosphate-buffered saline with 0.05% (w/v) Tween 80 (PBS-T) were spread onto LBT agar plates supplemented with appropriate antibiotics. For adaptation to hypoxia experiments, 100-ml serum vials were used, containing 30 ml of LBT or HdB. For iron limitation the iron chelator, ethylenediamine-*N*,*N*′-bis(2-hydroxyphenylacetic acid), was added to media at a final concentration of 10 μM, and to supplement the media with extra iron, iron sulfate was added to a final concentration of 100 μM. External pH of cultures was measured using pH indicator strips (4.0–7.0 or 7.5–14.0; Merck). Absorbance was measured at 600 nm (A_{600}) using culture samples diluted in saline to bring A_{600} to below 0.5 when measuring in cuvettes of 1-cm light path length in a Jenway 6300 spectrophotometer.

DNA Manipulation and Cloning of Constructs—Genomic DNA from *M. smegmatis* was isolated using the cetyltrimethylammonium bromide method (26). Restriction or DNA-modifying enzymes and other molecular biology reagents were obtained from Roche Diagnostics or New England Biolabs. All primers used in this study are shown in supplemental Table S1. The tetracycline-inducible expression construct for *mazF* was made by amplifying the gene using primers mazFpSE100 F and mazFpSE100 R. This product was ligated into the BamHI/PstI sites of pSE100 (27) (Addgene plasmid 17972), creating plasmid pRF202. This was also done for the *mazEF* operon using primers mazEFpSE100 F and mazFpSE100 R, and this created plasmid pRF203. Plasmids pRF202 and pRF203 were electroporated into mc^{2}155 with pMC1s (28), which integrates into the *attB* site. The primers docpMind F and docpMind R were used to amplify the *doc* gene, and this product was ligated into the BamHI/SpeI sites of pMind (29), creating pRF200. The *phd/doc* operon was amplified using primers phd/docpMind F and docpMind R. This product was also ligated into the BamHI/SpeI sites of pMind, creating pRF201.

To create a construct for the deletion of MSMEG_4447 and MSMEG_4448 (*mazEF*), PCR products of ~850 bp flanking the *mazEF* genes of *M. smegmatis* were amplified using the primer mazEFKOLF F with primer mazEFKOLF R (left flank) and primer mazEFKORF F with primer mazEFKO RF R (right flank). Primer mazEFKOLF R and primer mazEFKORF F contain 7-bp overlapping regions. The left flank and right flank PCR products were used in a second PCR with primer mazEFKOLF F and primer mazEFKORF R to generate an overlapping PCR product of the *mazEF* flanking regions with 88% of the genes deleted. This PCR product was digested with SpeI and ligated into the SpeI site of the pBluescript II KS plasmid. The insert was then subcloned into pX33 (30) generating the pRF220 plasmid. Allelic replacement was carried out essentially as described previously (31, 32); it was achieved by growing a culture of *M. smegmatis* carrying pRF220 in Middlebrook 7H9-ADC medium with gentamicin at 28 °C with agitation (200 rpm) to an A_{600} of ~0.5, followed by plating on LBT plates with gentamicin and incubating at 40 °C. Incubation at 40 °C selected for integration of the entire deletion construct into the chromosome of *M. smegmatis* via a single crossover event at either the left or right flank. Colonies that formed a yellow

TABLE 1
Bacterial strains and plasmids used in this study

	Description[a]	Source or ref.
Bacterial strains		
E. coli		
DH10B	F$^-$ *mcrA*Δ(*mrr-hsdRMS-mcrBC*) ϕ80d*lacZ*ΔM15 Δ*lacX74deoRrecA1 araD139*Δ(*araleu*)*7697galUgalKrpsLendA1nupG*	77
M. smegmatis		
mc^{2}155	Electrocompetent wild-type strain of *M. smegmatis*	78
RF100	mc^{2}155Δ*mazEF*	This study
RF101	mc^{2}155Δ*phd/doc*::*aphA-3*; Km^r	This study
RF102	mc^{2}155Δ*mazEF*Δ*vapBC*::*aphA-3*; Km^r	This study
RF103	mc^{2}155Δ*mazEF*Δ*phd/doc*::*aphA-3*; Km^r	This study
RF104	mc^{2}155Δ*vapBC*::*aphA-3*Δ*phd/doc*::*aphA-3*; Km^r	This study
RF105	mc^{2}155Δ*mazEF*Δ*vapBC*::*aphA-3*Δ*phd/doc*::*aphA-3*; ΔTA^{triple}; Km^r	This study
RF121	mc^{2}155 with pRF211 integrated in *attB*; Strep^r	This study
RF122	RF101 with pRF211 integrated in *attB*; Km^r Strep^r	This study
Plasmids		
pBluescript II KS	Cloning vector; Ap^r	Stratagene
pUC18K	*E. coli* plasmid containing an excisable, nonpolar kanamycin resistance cassette; Km^r Ap^r	33
pX33	*E. coli*-mycobacteria shuttle vector for allelic exchange mutagenesis in mycobacteria, pPR23, carrying a constitutive *xylE* marker; Gm^r Sac^s ts	30
pSM128	*lacZ* transcriptional fusion vector derived from pYUB, with mycobacteriophage L5 integrase and *attP* for integration into *attB* of mycobacteria; Spec^r Strep^r	35
pJEM15	*E. coli*-mycobacteria shuttle vector for the creation of transcriptional promoter fusions to *lacZ*; Km^r	34
pMind	Tetracycline-inducible expression vector; Km^r Hyg^r	29
pSE100	Tetracycline-inducible expression vector; Hyg^r	27; Addgene 17972
pMC1s	Tetracycline repressor under strong mycobacterial promoter; Km^r	28; Addgene 17969
pJR113	pX33 harboring Δ*vapBC*::*aphA-3*; Km^r Gm^r Sac^s ts	22
pRF202	pSE100 harboring *mazEF* with RBS from kanamycin marker; Hyg^r	This study
pRF203	pSE100 harboring *mazF* with RBS from kanamycin cassette; Hyg^r	This study
pRF200	pMind harboring *doc* with RBS from kanamycin marker; Km^r (Hyg^r)	This study
pRF201	pMind harboring *phd/doc* with RBS from kanamycin marker; Km^r (Hyg^r)	This study
pRF210	pJEM15 harboring a 663-bp *PmazE-lacZ* fusion; Km^r	This study
pRF211	pSM128 harboring a 576-bp *Pphd-lacZ* fusion; Spec^r Strep^r	This study
pRF220	pX33 harboring Δ*mazEF*; Gm^r Sac^s ts	This study
pRF221	pX33 harboring Δ*phd/doc*::*aphA-3*; Km^r Gm^r Sac^s ts	This study

[a] The following abbreviations are used: Gm^r, gentamicin resistance; Hyg^r, hygromycin B resistance; Km^r, kanamycin resistance; Ap^r, ampicillin resistance; Strep^r, streptomycin resistance; Spec^r, spectomycin resistance; Sac^s, sucrose sensitivity; ts, temperature sensitivity.

product when exposed to 250 mM catechol because of the presence of the *xylE* marker were screened by Southern hybridization analysis for correct integration of the construct. One integrant was chosen and grown in LBT with gentamicin at 37 °C, 200 rpm to an A_{600} of ~0.5, followed by plating onto low salt LBT plates (2 g of NaCl liter^{-1}) containing 10% sucrose and incubated at 40 °C to select for a second crossover event resulting in loss of the plasmid and replacement of *mazEF* with the overlapping flanks. Colonies that did not form the yellow product after exposure to catechol were picked onto LBT plates to confirm loss of the plasmid backbone. Candidate clones were screened by Southern hybridization analysis for correct deletion of *mazEF*. Replacement of *mazEF* with the overlapping flanks created strain RF100 (Δ*mazEF*).

To create a construct for the deletion of MSMEG_1277 and MSMEG_1278 (*phd/doc*), the kanamycin resistance (Km^r) cassette, encoded by *aphA-3*, was amplified from pUC18K (33) by using primers 5′mcspUC F and 3′mcspUC R. The resulting 850-bp product was digested with EcoRI and PstI. PCR products of ~1000 bp flanking the *phd/doc* genes of *M. smegmatis* were amplified by using the primer phd/docKOLF F with primer phd/docKOLF R (left flank) and primer phd/docKORF F with primer phd/docKORF R (right flank). The left flank PCR product was digested with SpeI and EcoRI, and the right flank PCR product was digested with PstI and SpeI. Both flanking products and the kanamycin cassette were ligated into the SpeI site of the pBluescript II KS plasmid. The resulting assembly, left flank/Km^r/right flank, was subcloned as a SpeI fragment into pX33 (30) generating the pRF221 plasmid. The expected double crossover event would result in a nonpolar deletion insertion at the *phd/doc* locus, eliminating 73% of the *phd/doc* coding sequence in exchange for the kanamycin resistance marker. Allelic replacement of *phd/doc* was carried out essentially as described previously (32) and was achieved by growing a culture of *M. smegmatis* carrying pRF221 in Middlebrook 7H9-ADC medium with kanamycin at 28 °C with agitation (200 rpm) to an A_{600} of ~0.5, followed by plating onto low salt LBT plates (2 g NaCl liter^{-1}) containing kanamycin and 10% sucrose at 40 °C, selecting for double crossover events. Replacement of *phd/doc* with the kanamycin marker created strain RF101 (Δ*phd/doc*::*aphA-3*).

To create a Δ*mazEF* Δ*vapBC* Δ*phd/doc* triple mutant, a Δ*mazEF* Δ*vapBC* double mutant was made. Strain RF100 was transformed with pJR113 (22), and the mutant was created as described previously, and this is strain RF102. This strain was then transformed with pRF221, and the triple mutant (ΔTA^{triple}; RF105) was created using the two-step crossover protocol. All crossover events were analyzed by Southern hybridization. For Southern hybridization analysis, EcoRI-digested genomic DNA (SmaI-digested genomic DNA was used for the creation of the Δ*mazEF* Δ*vapBC* double mutant) of the putative mutants was separated on a 0.8% agarose/Tris acetate/EDTA gel and transferred onto a nylon membrane (Hybond-N$^+$; Amersham Biosciences) by vacuum blotting. Probes were labeled using Gene Images AlkPhos Direct Labeling and Detection System (Amersham Biosciences).

To create a transcriptional fusion of the *mazEF* operon, a PCR product encompassing 556 bp of DNA upstream of *mazE* and 107 bp of its coding region was amplified using the primers mazElac F and mazElac R. The product was cloned into the BamHI and Asp-718 sites of pJEM15 (34), creating plasmid pRF210. To create a transcriptional fusion of the *phd/doc* operon, a PCR product encompassing 330 bp of DNA upstream of *phd* and 96 bp of its coding region was amplified using the primers phdlac F and phdlac R. The product was cloned into the ScaI site of pSM128 (35), creating plasmid pRF211. The orientation of the insert was checked using primers phdlac F and 3′mcspUC R. This plasmid was then electroporated into *M. smegmatis* mc^{2}155 and strain RF101, creating strains RF121 and RF122, respectively. β-Galactosidase assays were carried out as described previously (22).

Conditional Expression of Toxins in M. smegmatis—Initial starter cultures of appropriate strains were grown in LBT to an A_{600} between 0.2 and 0.4 and used to inoculate a second starter culture in HdB medium. HdB starter cultures were then grown to an A_{600} between 0.1 and 0.2 and used to dilute 100 ml of HdB medium in a 500-ml flask to an A_{600} of 0.001. All media were supplemented with kanamycin (for *doc* and *phd/doc* expression with pMind) or with kanamycin and hygromycin (for *mazF* and *mazEF* expression with pSE100 and pMC1s). For all strains, growth was monitored until an A_{600} of between 0.1 and 0.15 was reached, and expression was induced with tetracycline HCl (20 ng ml^{-1}). Cell viability was measured over time, and dilutions were spread onto LBT agar containing the appropriate antibiotics and incubated for 3 days at 37 °C to monitor the effects of expression on growth. Each experiment was performed in triplicate with triplicate plates at each time point. To see the effect of expression on solid medium, each strain was streaked onto an agar plate supplemented with kanamycin (for *doc* and *phd/doc* expression with pMind) or with kanamycin and hygromycin (for *mazF* and *mazEF* expression with pSE100 and pMC1s), with or without tetracycline to induce expression of either the toxin or the antitoxin-toxin genes. Images of the plates were taken after 3 days of growth at 37 °C using a Gel Logic 200 Imaging System (Eastman Kodak Co.).

RNA Extraction and Reverse Transcriptase (RT)-PCR—RNA was extracted from 5 ml of broth culture grown to an A_{600} of 0.5 in LBT medium. Cells were harvested by centrifugation (16,000 × *g*, 1 min) and resuspended in 1 ml of TRIzol reagent (Invitrogen). Total RNA was extracted according to the manufacturer's instructions. Cells were ruptured with three rounds of bead beating in a Mini BeadBeater (Biospec; 5,000 rpm, 30 s). Contaminating DNA was removed from samples using 2 units of RNase-free DNase from a Turbo DNA-free kit (Ambion) according to the manufacturer's instructions. RNA concentrations were determined using a Nanodrop ND-1000 spectrophotometer. RNA quality was assessed by agarose gel electrophoresis. For the *mazEF* system, the RT-PCRs were performed with the primers mazRT-PCR2 F and mazRT-PCR3 R (Table S1) to determine whether *mazE* and *mazF* were co-transcribed and with primers mazRT-PCR1 F and mazRT-PCR3 R (Table S1) to detect a potential MSMEG_4446-*mazEF* transcript. For the *phd/doc* system, the RT-PCRs were performed with the primers docRT-PCR2 F and docRT-PCR3 R (Table S1) to determine whether *phd* and *doc* were co-transcribed, the primers docRT-PCR1 F and docRT-PCR3 R (Table S1) to determine

whether there is a MSMEG_1276-*phd/doc* transcript, and the primers docRT-PCR2 F and docRT-PCR4 R (Table S1) to detect a potential *phd/doc*-MSMEG_1279 transcript. The Titan One Tube RT-PCR system (Roche Diagnostics) was used according to the manufacturer's instructions. The RT step was carried out with 200 ng of RNA as the template at 42 °C for 30 min, followed by 30 cycles of PCR. Control reactions, with 200 ng of RNA or 150 ng of genomic DNA of *M. smegmatis* as template, were performed using *Taq* DNA polymerase (Roche Diagnostics) according to the manufacturer's instructions.

Determination of Transcriptional Start Site (TSS)—The transcriptional start sites of the *mazEF* and *phd/doc* operons was mapped by 5′-RACE using components of the 3′-/5′-RACE kit (Roche Diagnostics) according to the manufacturer's instructions. For the *mazEF* operon, the first strand cDNA was synthesized from 4 μg of total RNA of *M. smegmatis* with the *mazF*-specific primer mazF RACE1 R. The resulting cDNA was purified and dA-tailed following the kit instructions. Purified dA-tailed cDNA was then used as a template for PCR using the oligo(dT)-anchor primer and the *mazF*-specific primer mazRT-PCR3 R. This reaction was then used as the template for a second PCR using the PCR adaptor primer and the *mazE*-specific primer mazE RACE2 R. This product was gel-extracted and cloned into pGEM-T Easy (Promega) according to the manufacturer's instructions. Several clones were selected and sent for sequencing (using pGEM-T Easy primers T7 and SP6), and the last nucleotide before the poly(A) tail to align with the genome sequence was chosen as the most likely TSS. This same procedure was also followed for the *phd/doc* operon. First strand cDNA was synthesized with the *doc*-specific primer docRT-PCR3 R. The first PCR was with the *doc*-specific primer doc RACE1 R, and the second PCR was with the *phd*-specific primer phd RACE2 R.

Biochemical Assays and Stress Experiments—Stress experiments were performed with mid-exponential phase (A_{600} 0.2–0.3) cultures grown in LBT medium. For heat shock (55 °C), the cultures were placed at the indicated temperature without further manipulation. For acid and alkaline stress, the cells were collected by centrifugation (6,000 × *g*, 15 min) and resuspended in an equal volume in LBT (pH 7), acidified LBT (pH 4), or alkaline LBT (pH 9). For oxidative iron chelation and antibiotic stress, the respective compounds were added directly to the mid-exponential phase culture. Cultures were incubated under stress conditions at 37 °C with agitation (200 rpm). Samples were taken before the stress and 2 h after. Dilutions of each sample were spread onto agar plates to determine the amount of survival. All stress experiments were carried out in triplicate using triplicate plates at each time point. Live/dead staining of cultures of wild type and ΔTA^{triple} (RF105) were performed by staining with propidium iodide and SYBR Green I (both from Invitrogen) during growth in LBT. Samples were incubated for 15 min in the dark before analysis by epifluorescence microscopy (Olympus BX51) equipped with a ×100 magnification lens and a bandpass filter at (520 ± 30 nm).

The internal pH of cells was measured as described previously (36), with the following modifications. Samples of cultures were incubated with [^{14}C]methylamine hydrochloride (56 mCi/mmol, 2 μM final concentration) at 37 °C for 5 min. The cultures were then centrifuged through silicon oil (BDH Laboratory Supplies) in 1.5-ml microcentrifuge tubes (16,000 × *g*, 5 min), and 20 μl of the supernatant was removed. The tubes and contents were frozen (−80 °C), and the cell pellets were removed with dog nail clippers. Supernatant and cell pellets were dissolved in scintillation fluid, and the activity of [^{14}C]methylamine was counted using an LKB Wallac 1214 Rackbeta liquid scintillation counter (PerkinElmer Life Sciences). For the determination of $\Delta\Psi$, cells from batch cultures were added immediately to a glass tube containing [^{3}H]methyltriphenylphosphonium iodide (TPP^+) (30–60 Ci/mmol) and [^{3}H]TPP^+ (2.4 nM final concentration). After incubation for 5 min at 37 °C, the cultures (900 μl in triplicate) were filtered rapidly through a 0.45-μm cellulose acetate filter (Sartorius) as adapted from Zilberstein *et al.* (37). The filters were washed twice with 2 ml of 100 mM LiCl and dried for 60 min at 40 °C. Filters were resuspended in 2 ml of scintillation liquid and counts/min determined using an LKB Wallac 1214 Rackbeta liquid scintillation counter (PerkinElmer Life Sciences). The intracellular volume (3.45 μl mg of protein^{-1}) was determined previously (36). The $\Delta\Psi$ across the cell membrane was calculated from the uptake of [^{3}H]TPP^+ according to the Nernst relationship. Nonspecific [^{3}H]TPP^+ binding was estimated from cells that had been treated with a combination of ionophores, valinomycin and nigericin (20 μM final concentration of each compound), for 20 min prior to addition of [^{3}H]TPP^+.

Supernatant samples of wild type and RF105 were collected during long term survival to measure external ammonia. The assay is based on the method used by Horn and Squire (38); samples were mixed with phenate reagent (25 g/liter NaOH, 100 ml/liter phenol, and 0.25 g/liter sodium nitroferricyanide) and hypochlorite reagent (household bleach diluted 1:10 and pH adjusted to 6.5–7.0). Ammonium chloride was used for the standard. Absorbance was measured at 630 nm after 5 min of incubation at ambient temperature. The intracellular K^+ concentrations of wild type and ΔTA^{triple} (RF105) cultures were determined as described previously (39), with the following modifications. Cell pellets and supernatant samples were collected and digested with 3 M HNO_3 (ambient temperature, overnight). Debris was removed by centrifugation (16,000 × *g*, 10 min), and the K^+ concentration was determined with a flame photometer (Cole-Palmer 2655-00 Digital Flame Analyzer).

ATP was extracted from the cells by perchloric acid and $KOH/NaHCO_3$ treatment after separation of the cells from the growth medium as described previously (40) and frozen at −80 °C. Prior to analysis, samples were thawed, and the potassium perchlorate was removed by centrifugation (16,000 × *g*, 5 min, 4 °C). The ATP concentration was determined by the luciferin/luciferase method (41). Light output was measured with a luminometer (model FB12, EG&G Berthold) using ATP as a standard. Intracellular inorganic phosphate concentrations of wild type and ΔTA^{triple} (RF105) cells were measured as described previously (42). Samples were diluted to be within the linear range of the assay, and a standard containing up to 100 nmol of P_i was assayed at the same time. Development reagent (1% SDS, 10 mM ammonium molybdate, 0.6 M H_2SO_4 and 1.6% sodium ascorbate) was added to the sample, and after 10 min of incubation at ambient temperature the A_{750} was measured.

Microarray Analysis—Samples of wild type and ΔTA^{triple} (RF105) cultures grown on LBT aerobically were harvested from cultures incubated for 1 and 5 days for microarray analysis as described previously (43), and the arrays were performed as described previously (44). Quantitative real time PCR (qPCR) was performed as described previously (44).

Sample Preparation and GC-MS Analysis—Cultures of wild type and ΔTA^{triple} (RF105) were grown aerobically in LBT medium, and samples for metabolomic analysis were collected after 15 days of incubation. Samples were then processed as described in Smart *et al.* (45). The samples were quenched by rapidly transferring 50 ml of the microbial culture into Falcon tubes containing 150 ml of a precooled (−20 °C) solution of cold glycerol/saline. The quenched samples were quickly homogenized followed by 5 min of acclimatization in cold ethanol bath (−20 °C). For the analysis of extracellular metabolites, 10 ml of culture was filtered through a 0.2-μm syringe filter to remove microbial cells. Then the samples were separated into 3 aliquots of 1 ml each, and 20 μl of internal standard (L-alanine-2,3,3,3-d_4 10 mM) was added to each aliquot. The samples were then freeze-dried using a 12-liter Labconco freeze dryer (Labconco Corp.). For the analysis of intracellular metabolites, the quenched samples were centrifuged at 36,086 × *g* for 20 min at −20 °C to separate the microbial cells from the extracellular medium. The supernatants were discarded, and the cell pellets were submitted to metabolite extraction as described in Smart *et al.* (45). Before extraction, 20 μl of internal standard (L-alanine-2,3,3,3-d_4 10 mM) was added to each sample. The freeze-dried samples containing extra- and intracellular metabolites were then resuspended in 200 μl of sodium hydroxide solution (1 M) and derivatized according to Smart *et al.* (45). The derivatized samples were analyzed using a gas chromatography-mass spectrometry (GC-MS) system (GC7890 coupled to a MSD5975, Agilent Technologies), with a quadrupole mass selective detector (EI) operated at 70 eV. The column used for all analyses was a ZB-1701 (Phenomenex), 30 × 250 m (internal diameter) × 0.15 (film thickness), with a 5-m guard column. The MS was operated in scan mode (start after 6 min; mass range 38–650 atomic mass units at 1.47 scans/s (45).

Metabolomics Data Analysis—The main objective of this study was to compare the metabolite profiles generated by the wild-type strain mc^{2}155 of the bacteria *M. smegmatis* and ΔTA^{triple} (RF105). The results produced by the GC-MS were processed according to Smart *et al.* (45) using the R package Metab (46). The samples were analyzed by the automated mass spectral deconvolution and identification system, which deconvolutes and identifies GC-MS peaks using an in-house MS library. The final relative concentration of metabolites was determined using the GC peak intensity of methyl chloroformate derivatives. Compounds considered false-positives were then eliminated, and the intensity of each metabolite was normalized by the peak height of the internal standard (L-alanine-d_4). Because the amount of biomass was identical between replicates, no normalization by biomass was performed. Extracellular samples were additionally normalized by the relative abundance of metabolite identified in the uncultured medium. Finally, the data were log-transformed to fit the normal distribution criteria, and *t* test or analysis of variance was performed to highlight compounds showing significantly (p value < 0.05) different relative abundances between conditions.

RESULTS

M. smegmatis mc^{2}155 Contains Homologs of MazEF and Doc/Phd Toxin-Antitoxin Modules—*M. smegmatis* mc^{2}155 contains one *vapBC* toxin-antitoxin module (22) and two other putative TA operons, *mazEF* and *phd/doc* (19). MazF from *M. smegmatis* (MSMEG_4448) is a member of the PemK superfamily (NCBI annotation = transcriptional modulator of MazE; Pfam number = PF02452), which currently contains 1393 proteins from 376 species of bacteria and archaea. Proteins that share the highest amino acid sequence with *M. smegmatis* MazF are found in *Mycobacterium avium* subsp. *paratuberculosis* K-10 (MAP_2085, 73% sequence identity), *Rhodococcus jostii* RHA1 (RHA1_ro08517, 65% sequence identity), and *Rhodopseudomonas palustris* BisB18 (RPC_0821, 58% sequence identity). The antitoxin MSMEG_4447 (*mazE*) does not have any similarity to other *mazE* genes. It is annotated as a conserved hypothetical protein, and is a protein of unknown function (DUF3018). Proteins that share the highest sequence identity with *M. smegmatis* MazE are found in *R. jostii* RHA1 (RHA1_ro08516, 85% sequence identity) and in the *M. tuberculosis* strains CDC1551, H37Ra, and F11 (MT_2721, MRA_2673, and TBFG_12662, respectively, 81% sequence identity). This region of the chromosome appears to be conserved in these *M. tuberculosis* strains with an arsenic transport system upstream.

Doc from *M. smegmatis* (MSMEG_1278) is a member of the Fic superfamily (NCBI annotation = death-on-curing protein; Pfam number = PF02661), which contains proteins from all three kingdoms (20), and has the conserved residues HPF*XX*GNG. Proteins that share the highest sequence identity with *M. smegmatis* Doc are found in other mycobacterial species, *Mycobacterium* sp. MCS (Mmcs_0835, 89% sequence identity), *Mycobacterium* sp. KMS (Mkms_0853, 88% sequence identity), and *Mycobacterium kansasii* ATCC 12478 (MkanA1_11399, 71% sequence identity); however, there are no antitoxin-like genes annotated upstream of these toxins. The antitoxin Phd from *M. smegmatis* (MSMEG_1277) is annotated as a hypothetical protein and shares low sequence similarity with hypothetical proteins from *M. kansasii* ATCC 12478 (MkanA1_11394, 62% sequence identity) and *Microbacterium* sp. MA1 (58% sequence identity).

Conditional Expression of MazF Causes Cell Death of M. smegmatis—MazF toxins found on the chromosomes of different bacteria have varying levels of toxicity when overexpressed and usually have a bactericidal effect (21, 47–51). To determine whether the MazF toxin had a similar effect in *M. smegmatis*, pRF202 was constructed with the *mazF* gene under the control of a tetracycline-inducible promoter, and the tetracycline repressor gene, *tetR*, is encoded on the integrative vector pMC1s (Table 1). To ensure the effect observed was due to the production of MazF alone, the operon *mazEF* was also cloned in the same manner, creating pRF203, thus preventing the

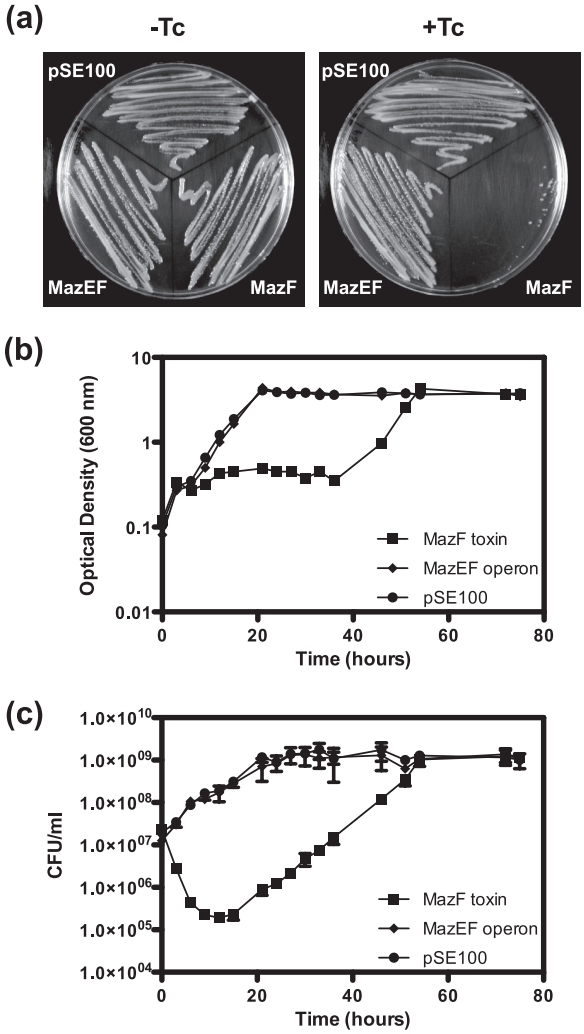

FIGURE 1. **Effect of MazF on growth and viability of *M. smegmatis*.** *a*, *M. smegmatis* wild type harboring plasmid pSE100 (empty vector), pSE100-*mazF* (expressing the MazF toxin, pRF202), or pSE100-*mazEF* (expressing the MazEF operon, pRF203) with or without tetracycline (*Tc*). *M. smegmatis* wild type harboring plasmid pSE100, pSE100-*mazF* (pRF202), or pSE-*mazEF* (pRF203) was grown in HdB medium supplemented with hygromycin and kanamycin at 37 °C until an A_{600} of 0.1–0.15. Induction of expression at 0 h was by the addition of Tc (final concentration 20 ng ml^{-1}). *b*, cellular growth (A_{600}). *c*, cellular viability (cfu/ml) shown as the mean ± S.D. of technical replicates of each time point. Results are representative of three independent experiments.

effect of the toxin by co-expressing the cognate antitoxin. Both constructs were placed into *M. smegmatis* mc^{2}155 with pMC1s, which integrates into the *attB* site (28). The empty vector, pSE100, was used as a control. In the presence of tetracycline, cells expressing MazF could not grow on an agar plate, although cells expressing the antitoxin MazE as well as MazF were able to grow (Fig. 1*a*, *right panel*). All three strains could grow normally on agar plates without tetracycline (Fig. 1*a*, *left panel*). A toxic effect was also seen in liquid culture (Fig. 1*b*). Cultures were induced at an A_{600} between 0.1 and 0.15 and were then monitored by A_{600} and cell viability (cfu) measurements. *M. smegmatis* mc^{2}155 expressing MazF decreased in cfu ml^{-1} by 2 orders of magnitude 12 h after induction (Fig. 1*c*). No effect was seen on cell growth when MazEF was expressed compared with the empty vector control strain (Fig. 1, *b* and *c*). Regrowth of the culture expressing MazF was seen after 22 h of induction. To address the molecular basis for regrowth, we sequenced the plasmid DNA from these cultures. This analysis revealed that these strains harbored plasmids in which deletions were detected in either the *mazF* gene or the Tc promoter region (data not shown).

M. smegmatis mazEF Is Transcribed as a Single Leaderless mRNA and Autoregulated by MazEF Complex—The *mazEF* genes of *M. smegmatis* are organized in a manner that suggests they could be transcribed as a single operon, with a 3-bp gap between *mazE* and *mazF* (Fig. 2*a*). To confirm this operon structure, RT-PCR was performed with primers that bound within the *mazEF* genes (Fig. 2*a*, primers 2 and 3). A single 443-bp RT-PCR product was obtained (Fig. 2*b*, *lane 4*), and sequencing confirmed that *mazEF* of *M. smegmatis* is a bicistronic message. The open reading frame MSMEG_4446 lies upstream of the *mazEF* operon and is in the same orientation; to investigate whether this gene is also part of the operon, another set of primers was used (Fig. 2*a*, primers 1 and 2). No product representing an MSMEG_4446-*mazEF* transcript was obtained (Fig. 2*b*, *lane 2*). Positive controls were performed by PCR using template genomic DNA and products for both primer sets (1 and 2; 2 and 3) were obtained (Fig. 2*b*, *lanes 1* and *3*, respectively). To exclude DNA contamination in RNA preparations, PCR was performed without a preceding reverse transcriptase step, which resulted in no product (data not shown). To map the transcriptional start site of the *mazEF* operon, 5′-RACE analysis was performed. The transcriptional start site of *mazEF* was determined as the first nucleotide of the ATG start codon, based on trace data (data not shown), suggesting *mazEF* is transcribed as a leaderless mRNA.

A *promoter-mazE-lacZ* (hereafter *PmazE-lacZ*) transcriptional fusion was created (pRF210) consisting of 556 bp upstream of the *mazEF* transcriptional start site and 107 bp of the *mazE* coding region fused to *lacZ* (Fig. 2*d*). When the wild type containing *PmazE-lacZ* was grown under normal laboratory conditions, the expression of *PmazE-lacZ* was constitutive during exponential growth and early stationary phase; the β-galactosidase activity was in the range of 50–70 Miller units (MU), and in late stationary phase the promoter activity was reduced to around 20 MU (Fig. 2*e*, *top panel*).

The expression of TA modules has been reported to be regulated by the toxin-antitoxin complex (5). To study this phenomenon, a single deletion mutant of *mazEF* was created. The *mazEF* deletion mutant was created by allelic exchange mutagenesis (Fig. 2*c*). Eighty eight percent of the *mazEF* operon was deleted after the second crossover event; this was confirmed by Southern hybridization analysis (Fig. 2*c*). EcoRI-digested genomic DNA of the wild type produced a 1.4-kb band when probed with the left flank after the first crossover event. When the pRF220 construct had integrated through the right flank, two bands were detected, one 1.4 kb and the other 4.8 kb (Fig. 2*c*). The deletion mutant had a single band of 2.2 kb, confirming that the plasmid had been removed from the genome correctly. This mutant was designated strain RF100. When expression of *PmazE-lacZ* was measured in the *mazEF* deletion strain background, the level of β-galactosidase activity in exponential and early stationary phase was in the range of 60–110

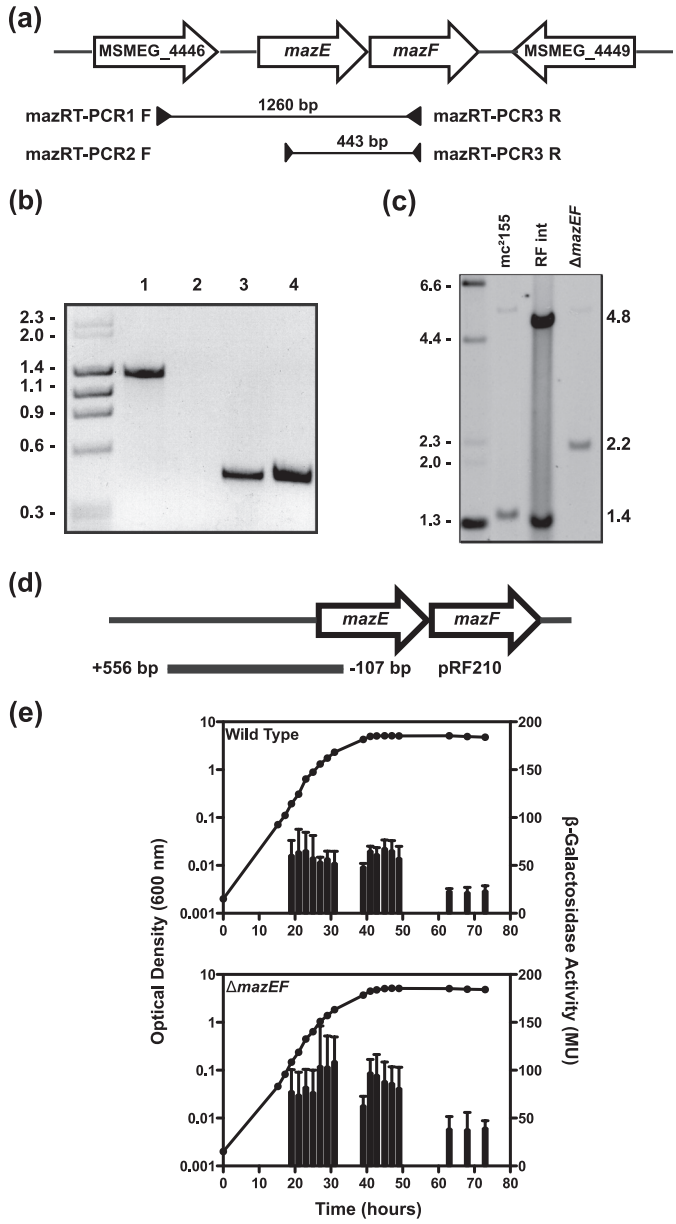

FIGURE 2. **Genetic organization and promoter activity of *mazEF*.** *a,* schematic of the *mazEF* genomic region. *Open arrows* indicate the genetic organization of ORFs MSMEG_4447 (*mazE*) and MSMEG_4448 (*mazF*), as well as the upstream gene MSMEG_4446 (annotated as a dihydrolipoamide dehydrogenase) and the downstream gene MSMEG_4449 (annotated as a putative transcriptional regulator). Amplified regions and the primers used are indicated *below* the ORFs. *b,* electrophoresed bands from RT-PCRs using primers 1 and 2 (*lane 2*) and primers 2 and 3 (*lane 4*). PCR-positive controls use genomic DNA and primer pairs 1 and 2 (*lane 1*) and primer pairs 2 and 3 (*lane 3*). Molecular weight standards indicated in kb are shown on the *left*. *c,* replacement of the *mazEF* operon was screened by Southern hybridization analysis. EcoRI-digested genomic DNA from wild-type mc^{2}155, a right flank integrant, and the *mazEF* deletion strain RF100 was probed with left flank PCR product. Molecular weight standards indicated in kb are shown on the *left*. *d,* diagram of the *PmazE-lacZ* fusion construct pRF210, indicating the position of the insert cloned into the episomal vector in relation to the *mazEF* genes. The base pairs indicated are relative to the TSS (+1) identified by 5′-RACE. *e, M. smegmatis* wild type and the Δ*mazEF* strain (RF100) were grown in LBT (*closed circles*), and β-galactosidase activity (*vertical bars*) was measured (mean ± S.D. of technical assays performed on each sample). Results shown are representative of three independent experiments.

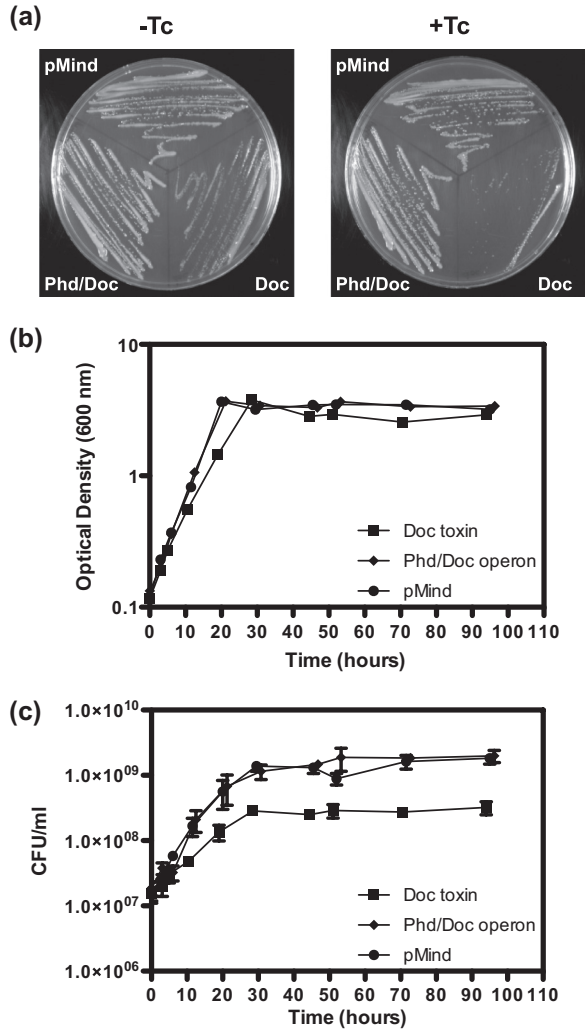

FIGURE 3. **Effect of Doc on growth and viability of *M. smegmatis*.** *a, M. smegmatis* wild type harboring plasmid pMind (empty vector), pMind-*doc* (expressing Doc toxin, pRF200), or pMind-*phd/doc* (expressing Phd/Doc operon, pRF201) with or without Tc. *M. smegmatis* wild types harboring plasmid pMind, pMind-*doc* (pRF200), or pMind-*phd/doc* (pRF201) were grown in HdB medium supplemented with kanamycin at 37 °C until an A_{600} of 0.1–0.15. Induction of expression at 0 h was by the addition of Tc (final concentration 20 ng ml^{-1}). *b,* cellular growth. *c,* cellular viability shown as the mean ± S.D. of technical replicates of each time point. Results shown are representative of three independent experiments.

MU and decreased to around 40 MU in late stationary phase (Fig. 2*e*, *bottom panel*). This indicates that one or both MazEF proteins are required for some autoregulation of the *mazEF* operon. These data demonstrate the *mazEF* genes in *M. smegmatis* constitute a TA module.

Conditional Expression of Doc Causes Bacteriostasis of M. smegmatis—To determine whether overexpression of Doc had an effect on *M. smegmatis*, pRF200 was constructed with the *doc* gene under the control of a tetracycline-inducible promoter (29). The operon *phd/doc* was also cloned in the same manner to ensure that the effect seen was due to production of Doc alone, and this created pRF201. Both constructs were placed into the background of *M. smegmatis* mc^{2}155, and kanamycin was used for selection. As a control, the empty vector pMind was used. In the presence of tetracycline, cells expressing Doc were inhibited in their growth on agar plates, with only very small colonies being visible after 3 days of incubation (Fig. 3*a*, *right panel*), and growth of *M. smegmatis* harboring *doc* (− tetracycline) was slightly inhibited (Fig. 3*a*, *left panel*), but

pMind has been shown to be leaky (29). The strains harboring the *phd/doc* operon or the empty vector were able to grow normally on agar with or without tetracycline (Fig. 3*a*). The effect of expression in liquid culture was also investigated (Fig. 3, *b* and *c*). Cultures were induced at an A_{600} between 0.1 and 0.15 and were then monitored by A_{600} (Fig. 3*b*), and cell viability (cfu) measurements (Fig. 3*c*). *M. smegmatis* expressing Doc had a slower growth rate and entered stationary phase at a lower cfu ml^{-1} compared with the strains expressing Phd/Doc or harboring the empty vector (Fig. 3, *b* and *c*).

M. smegmatis Phd/Doc Is Transcribed as Part of a Larger Operon and Subject to Autoregulation by the Complex—The *phd/doc* genes of *M. smegmatis* are genetically organized like many other toxin-antitoxin systems where the upstream gene *phd* stop codon overlaps with the start codon of the downstream gene, *doc*, suggesting that these genes might be transcribed as an operon (Fig. 4*a*). To confirm that the *phd/doc* genes are co-transcribed, RT-PCR was performed with primers that bound within the *phd/doc* genes (Fig. 4*a*, primers 4 and 5). A single 470-bp RT-PCR product was obtained (Fig. 4*b*, *lane 2*), and sequencing confirmed that *phd/doc* is a bicistronic message. The upstream open reading frame, MSMEG_1276, is in the same orientation, so the RT-PCR was repeated with another set of primers, which spanned this gene and the *phd/doc* genes, to see if this gene is included in the operon (Fig. 4*a*, primers 5 and 6). A single 781-bp product was obtained (Fig. 4*b*, *lane 4*). Another RT-PCR was performed with primers that bound to *phd* and the downstream gene MSMEG_1279, as this gene is also in the same orientation (Fig. 4*a*, primers 4 and 7). A single 950-bp product was obtained (Fig. 4*b*, *lane 6*). Sequencing of both of these RT-PCR products confirmed that MSMEG_1276-*phd/doc*-MSMEG_1279 is part of a larger operon. Positive controls were performed by PCR using genomic DNA as the template, and products were obtained for all primer pairs, 4 and 5, 5 and 6, and 4 and 7 (Fig. 4*b*, *lanes 1, 3* and *5*, respectively). To exclude DNA contamination in RNA preparations, PCR was performed without a preceding reverse transcriptase step, which resulted in no product (data not shown).To map the transcriptional start site of the *phd/doc* operon, 5′-RACE analysis was performed. The transcriptional start site was determined as the adenyl nucleotide 6 bp after the translational start site given in the annotated genome (Fig. 4*c*). A *promoter-phd-lacZ* (hereafter *Pphd-lacZ*) transcriptional fusion was created (pRF211) consisting of 330 bp upstream of the *phd/doc* transcriptional start site, and 96 bp of the *phd* coding region fused to *lacZ* (Fig. 4*e*). This integrative construct was transformed into the wild-type strain creating RF121. When RF121 was grown under normal laboratory conditions, *Pphd-lacZ* expression was constitutive throughout the growth curve, and the β-galactosidase activity was in the range of 30–40 MU (Fig. 4*f*, *top panel*).

Using allelic exchange mutagenesis, 73% of the *phd/doc* genes were replaced with a nonpolar kanamycin resistance cassette (*aphA-3*) and confirmed this deletion by Southern hybridization analysis (Fig. 4*c*). The wild-type EcoRI-digested genomic DNA had a 10.9-kb band, when probed with the left flank, which was shifted to 4.5 kb in the deletion mutant due to the introduction of another EcoRI site from the kanamycin resistance cassette (Fig. 4*c*). This mutant was designated strain RF101. The *phd/doc* deletion strain containing pRF211 (RF122) showed a constitutive level of expression, but the β-galactosidase activity was in the range of 60–90 MU (Fig. 4*f*, *lower panel*), indicating that one or both proteins are required for repression of the *phd/doc* operon. Taken together, these data demonstrate that the *phd/doc* genes in *M. smegmatis* are a TA system.

Phenotypic Analysis of Individual TA Deletion Mutants and Construction of a vapBC-mazEF-phd/doc Triple Deletion Mutant—To study the role of the MazEF module in *M. smegmatis*, general growth characteristics of the strain RF100 (Δ*mazEF*) in comparison with the wild type were analyzed. The specific growth rates (h^{-1}) of the *mazEF* mutant and isogenic wild type were compared in LBT, HdB, and HdB limited for carbon, phosphate, or nitrogen, and no significant difference was observed (supplemental Table S2). To study the role of the Phd/Doc module in *M. smegmatis*, general growth characteristics of the strain RF101 (Δ*phd/doc*) in comparison with the wild type were analyzed. The growth rates of the *phd/doc* deletion mutant and isogenic wild type were compared in LBT, HdB, and HdB limited for carbon, phosphate, or nitrogen, and no significant difference was observed (supplemental Table S2).

We did not observe any significant phenotypic differences for the single Δ*mazEF* and Δ*phd/doc* mutants constructed in this study. To study the role of all three TA modules in *M. smegmatis*, we constructed a mutant in which all three TA modules were deleted. To create a triple deletion strain, a double *mazEF* and *vapBC* mutant was first constructed. Ninety six percent of the *vapBC* genes were replaced with the kanamycin resistance cassette in the Δ*mazEF* deletion strain, and this was confirmed by Southern hybridization (Fig. 5*a*) as in Robson *et al.* (22). This double mutant strain was designated strain RF102. The *phd/doc* genes were then replaced in strain RF102 with the kanamycin resistance cassette using a two-step protocol, and again this was confirmed by Southern hybridization analysis (Fig. 5*b*). This triple mutant, which has no TA modules, was designated strain RF105 and is referred to as ΔTA^{triple}. General growth characteristics of the triple deletion mutant ΔTA^{triple} (RF105), in comparison with the wild type, were analyzed. No significant differences in growth rate or the final absorbance reached were seen between the wild type and the ΔTA^{triple} mutant (strain RF105) when grown in LBT and HdB media (supplemental Table S2). Carbon, nitrogen, and phosphate limitation also showed no significant difference in growth rate between the wild type and the ΔTA^{triple} mutant (supplemental Table S2). Single deletion mutants Δ*mazEF* (RF100) and Δ*phd/doc* (RF101) showed similar growth characteristics to the wild type and ΔTA^{triple} mutant (supplemental Table S2).

M. smegmatis vapBC-mazEF-phd/doc Triple Deletion Mutant Is Defective in Survival in Complex Medium—TA modules have previously been linked to stress responses, where TA deletion strains have a survival advantage over wild-type strains. In the wild-type strains, the stress causes an imbalance between the level of antitoxin and toxin, resulting in free toxin, which is able to cause cell death. We therefore investigated if the TA modules of *M. smegmatis* were beneficial to an exponentially growing culture exposed to different stress conditions (Fig. 6*a*). No significant differences between ΔTA^{triple} (RF105)

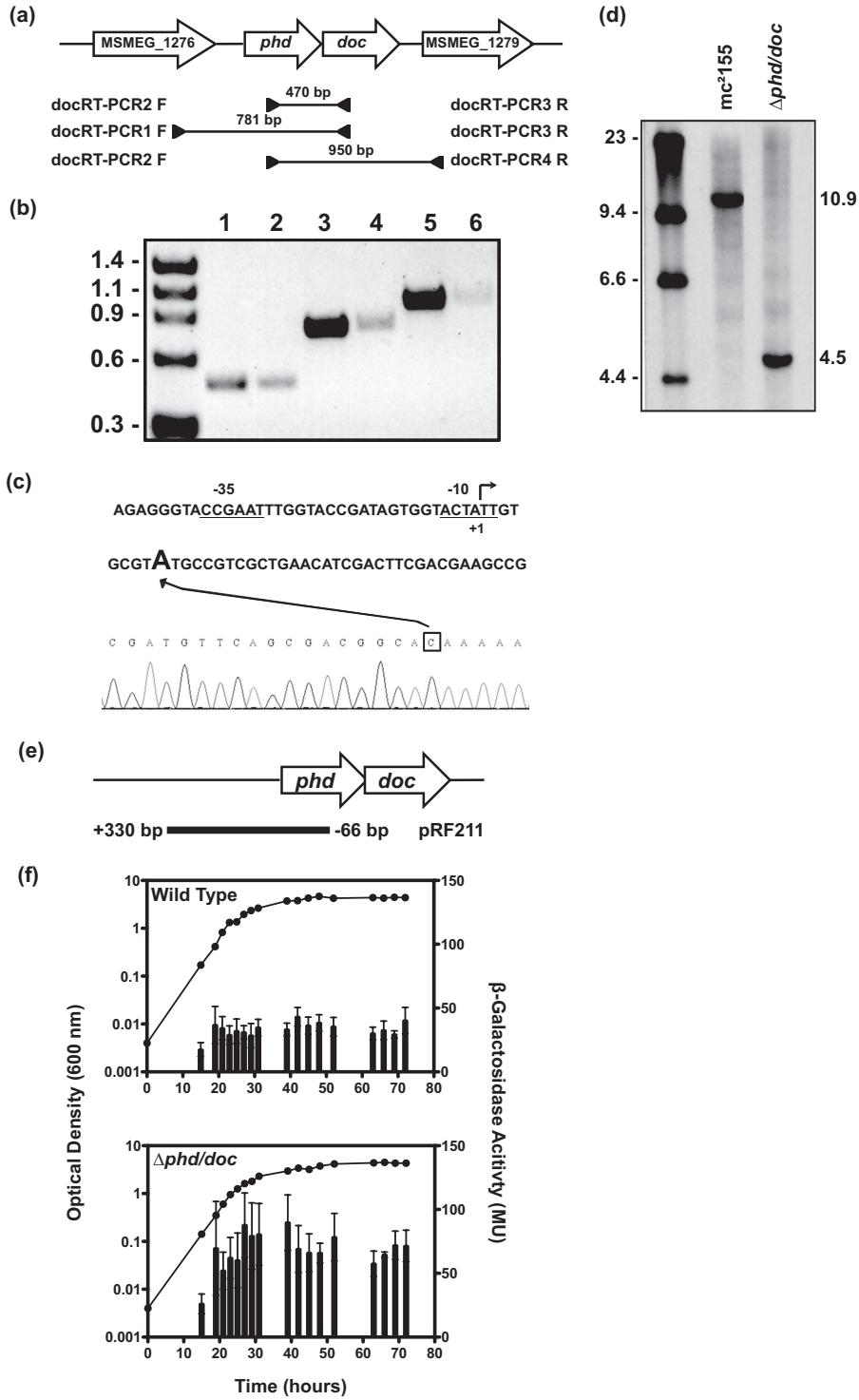

FIGURE 4. **Genetic organization and promoter activity of *phd/doc*.** *a,* schematic of the *phd/doc* genomic region. *Open arrows* indicate the genetic organization of ORFs MSMEG_1277 (*phd*) and MSMEG_1278 (*doc*), as well as the upstream gene MSMEG_1276 (annotated as a hypothetical protein) and the downstream gene MSMEG_1279 (annotated as a conserved hypothetical protein). Amplified regions and the primers used are indicated *below* the ORF. *b,* electrophoresed bands from RT-PCR using primers 4 and 5 (*lane 2*), primers 5 and 6 (*lane 4*), and primers 4 and 7 (*lane 6*). PCR-positive controls using genomic DNA for primer pair 4 and 5 (*lane 1*), primer pair 5 and 6 (*lane 3*), and primer pair 4 and 7 (*lane 5*). Molecular weight standards in kb are shown on the *left*. *c,* identification of the TSS of *phd/doc* operon. Schematic diagram showing the promoter region of the *phd/doc* operon indicating the translational start site (+1) as given by the annotated genome. The TSS was determined by 5′-RACE (*trace* is given in reverse sequence) and identifies the adenyl residue 6 bp downstream as the TSS. The *box* indicates the nucleotide C, which represents the A of the start codon for the *phd* gene. Putative −10 and −35 sequences are *underlined*. *d,* replacement of the *phd/doc* operon was screened by Southern hybridization analysis. EcoRI-digested genomic DNA from wild-type strain mc^{2}155 and *phd/doc* deletion strain RF101 was probed with left flank PCR product. *e,* diagram of the *Pphd-lacZ* fusion construct pRF211, indicating the position of the 426-bp region in relation to the *phd/doc* genes that was cloned into the integrative plasmid pSM128. The base pairs indicated are relative to the TSS (+1) identified by 5′-RACE. *f, M. smegmatis* wild type and Δ*phd/doc* strain (RF101), both harboring pRF211 (strains RF121 and RF122, respectively), were grown (*closed circles*) in LBT, and β-galactosidase activity (*vertical bars*) was expressed as the mean ± S.D. of technical assays performed on each sample. Results shown are representative of three independent experiments.

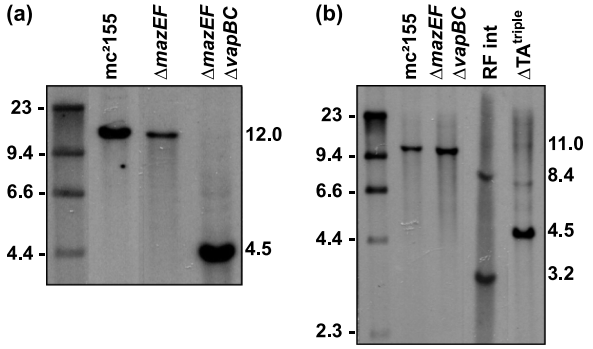

FIGURE 5. **Creation of a triple TA deletion mutant.** *a,* replacement of the *vapBC* operon with *aphA-3* in the Δ*mazEF* strain (RF100) was screened by Southern hybridization analysis. SmaI-digested genomic DNA from wild-type strain mc²155, Δ*mazEF* (RF100), and Δ*mazEF*Δ*vapBC* (RF102) was probed with left flank PCR. *b,* replacement of the *phd/doc* operon with *aphA-3* in the Δ*mazEF*Δ*vapBC* double deletion strain, RF102, was screened by Southern hybridization analysis. A two-step procedure was used as RF102 already contained the *aphA-3* marker. EcoRI-digested genomic DNA from wild-type strain mc²155, Δ*mazEF*Δ*vapBC* (RF102), right flank integrant strain, and Δ*mazEF*Δ*vapBC*Δ*phd/doc* triple deletion strain RF105 was probed with left flank PCR product labeled and detected as for RF102.

and the wild type were detectable after 2 h of exposure to the final concentrations of the following: rifampicin (80 mg ml^{-1}), streptomycin (2 mg ml^{-1}), ethylenediamine-*N*,*N*′-bis(2-hydroxyphenylacetic acid) (0.5 mM), mitomycin C (200 ng ml^{-1}), nalidixic acid (1 mg ml^{-1}), or exposure to acidic pH (pH 4) or alkaline pH (pH 9) as determined by viable cell counts (Fig. 6*a*). The only significant difference was observed for H_2O_2 (17.5 mM) and heat shock (55 °C), with the ΔTA^{triple} being more sensitive than the wild type (Fig. 6*a*). We attempted to isolate ΔTA^{triple} mutants (suppressor mutants) that were resistant to heat shock. This analysis was performed by plating cells at various temperatures 37, 40, 42, 45, and 50 °C and isolating ΔTA^{triple} mutants that grew at high temperature. No ΔTA^{triple} mutants could be isolated under these conditions that were resistant to heat shock. The percentage survival of wild type and ΔTA^{triple} was compared during long term survival under aerobic conditions in HdB (Fig. 6*b*) and in LBT (Fig. 6*c*). A significant and highly reproducible survival defect was seen under aerobic conditions using complex LBT medium, where the ΔTA^{triple} mutant did not survive past 15 days of starvation (Fig. 6*c*). The triple TA deletion mutant was the only mutant to have this pronounced survival defect compared with single and double deletion mutants (supplemental Fig. S1). Confirmation of this phenotype was demonstrated by live/dead staining with no viable cells in the ΔTA^{triple} mutant culture (Fig. 6*d*). The viability of the ΔTA^{triple} mutant and the wild type was tested under a number of culture conditions (supplemental Fig. S2). The ΔTA^{triple} mutant and the wild type did not show a significant difference in cell viability under the following conditions: self-induced hypoxia using either LBT or HdB (supplemental Fig. S2, *a* and *b*), exponential (supplemental Fig. S2, *c* and *d*) and stationary phase cells (supplemental Fig. S2, *e* and *f*) starved in PBS-T, and long term survival (25 days) in 7H9 and 7H9 + 10% ADC (supplemental Fig. S2*g*).

These data raised the question as to why the ΔTA^{triple} mutant could not survive long term starvation in complex medium. To gain molecular insight into this survival defect, we set out to isolate suppressor mutants of the ΔTA^{triple} mutant. Cells were starved for 25 days, and survivors (suppressor mutants) were plated (no dilution) onto agar plates incubated at various temperatures (25, 28, and 37 °C). Under no conditions could we isolate suppressor mutants to the survival defect of the ΔTA^{triple} mutant. This led us to investigate a number of cellular parameters required for cell viability (Fig. 7). It should be noted that at days 15–25 in LBT medium the external pH was ~9 (*i.e.* very alkaline), and this was due to the production of ammonia (60 mM). However, even at this very alkaline pH, the intracellular pH of the ΔTA^{triple} mutant was not compromised at days 20–25 where cell death was observed (Fig. 7*a*). The membrane potential was similar between the ΔTA^{triple} mutant and the wild type suggesting that the ability to generate a protonmotive force was not affected in the ΔTA^{triple} mutant (Fig. 7*b*). In accordance with the membrane potential data, we did not observe any significant difference in intracellular potassium concentration between the wild type and ΔTA^{triple} mutant suggesting critical ion homeostasis was unaffected in the ΔTA^{triple} mutant (Fig. 7*c*). The intracellular ATP concentration of the wild type and ΔTA^{triple} mutant decreased with days of starvation, but importantly there was no significant difference between the wild type and the mutant (Fig. 7*d*). The intracellular phosphate concentration did not vary significantly between the wild type and the mutant (Fig. 7*d*).

Transcriptional Profile of ΔTA^{triple} (RF105) Compared with Wild Type—To determine whether there was a transcriptional difference between the ΔTA^{triple} mutant and the wild type that caused the survival defect of the mutant in LBT, microarray analysis was performed on cells incubated for 1 and 5 days in LBT. We rationalized that the transcriptional response observed at these time periods would prepare the cells for surviving in LBT as the cells grew into stationary phase (see Fig. 6*c*). The microarray data from the cells grown in LBT for 1 day showed that a total of 19 genes were differentially expressed (p value < 0.05, expression ratio >2 or <0.5) in ΔTA^{triple} mutant compared with the wild type (supplemental Table S3). Of these 19 genes, 12 were up-regulated and 7 were down-regulated. After 5 days of growth in LBT, a total of 72 genes were differentially expressed (p value <0.05, expression ratio >2 or <0.5) in ΔTA^{triple} (RF105) compared with the wild type (supplemental Table S4). Of these 72 genes, three were up-regulated and 69 were down-regulated (supplemental Table S4). MSMEG_1280 and MSMEG_1282 were the only genes (Fig. 8*a*) that were significantly up-regulated in both the day 1 microarray analysis and in qPCR (Fig. 8, *b* and *c*). The qPCR did show that the *phd* antitoxin has been deleted from the chromosome of the triple TA deletion strain. In the microarray it appeared to be up-regulated, but this was due to the first 30 bp of the gene, which are still present in the deletion strain and are part of the oligonucleotide used on the microarray slide for *phd* (Fig. 8*b*). The gene with the highest fold change in expression level on day 1 in the ΔTA^{triple} mutant compared with wild type was MSMEG_1279, and this gene is predicted to be in an operon with MSMEG_1280, MSMEG_1281, and MSMEG_1282 (Fig. 8*a*), which were also up-regulated in this analysis. The *phd/doc* and *vapBC* TA systems flank these genes, and a schematic of this region of the chromosome is shown in Fig. 8*a,* and a heat map

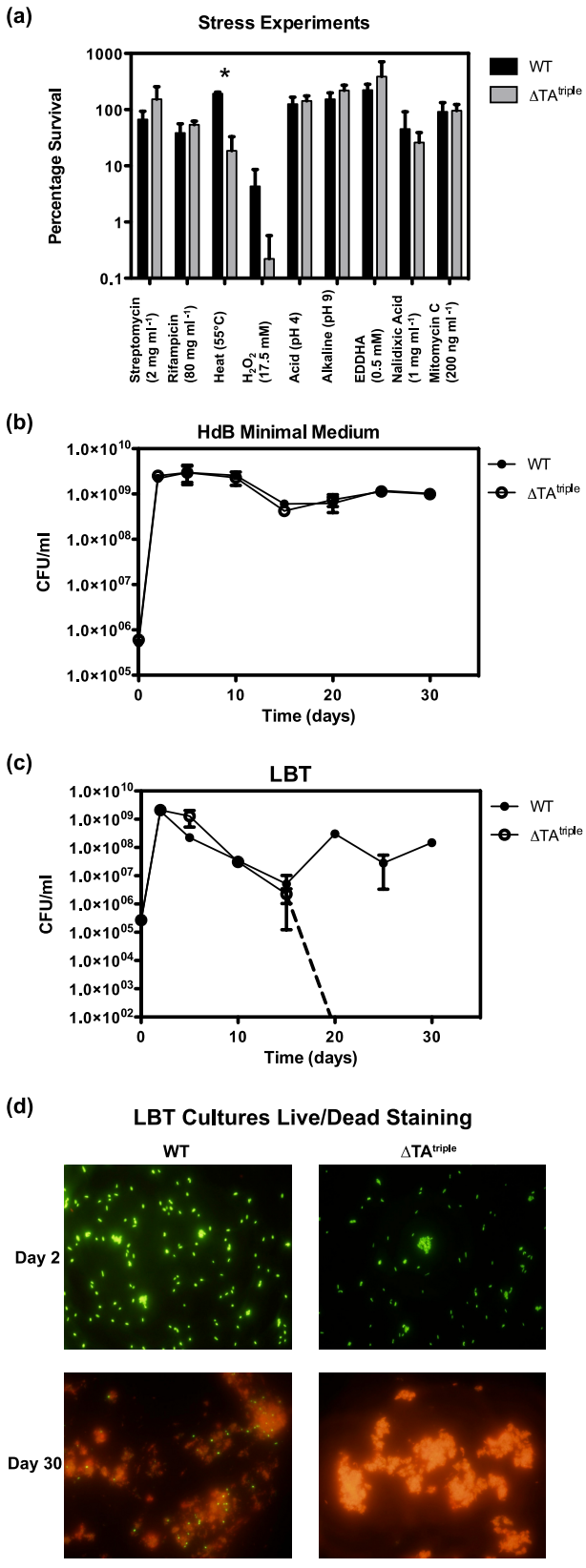

FIGURE 6. **Phenotypic analysis of triple TA deletion mutant Δ*mazEF*Δ*vapBC*Δ*phd/doc* (ΔTA^{triple}).** *a,* percentage survival of wild type and ΔTA^{triple} (RF105) was compared under various stress conditions in liquid culture. Mid-exponential phase cells were exposed to stress conditions as detailed under "Experimental Procedures." Viable cell counts were performed before the stress (100%) and after 2 h of exposure. Technical replicates were performed at each time point, and results shown are the mean ± S.D. for three independent experiments. *b,* long term survival of wild type and ΔTA^{triple} mutant (RF105) was measured in HdB over 30 days. Technical replicates were performed at each time point, and results shown are the mean ± S.D. for three independent experiments. *c,* long term survival of wild type and ΔTA^{triple} mutant was measured in LBT over 30 days. *Dotted line* indicates where cfu counts were no longer obtained for ΔTA^{triple} mutant. Technical replicates were performed at each time point, and results shown are the mean ± S.D. for three independent experiments. *d,* live/dead staining of wild type and ΔTA^{triple} mutant cells grown in LBT for 2 and 30 days.

showing the expression level from the transcriptomic analyses of these genes in ΔTA^{triple} (RF105) compared with wild type is shown in Fig. 8*b*. MSMEG_1280 was also significantly up-regulated in the day 5 transcriptomic analysis. The RT-PCR results from the *phd/doc* region suggest that MSMEG_1279 is co-transcribed with the *phd/doc* TA system, making it possible that MSMEG_1276–1282 form a large operon. As described above, it is not clear if MSMEG_1276 is part of this operon as its expression level is unchanged in the transcriptomic analyses, although the other genes are up-regulated (Fig. 8*b*) and the TSS was mapped to the start of *phd*. MSMEG_1279–1281 were annotated as hypothetical proteins, but a position-specific iterated (PSI) BLAST analysis revealed that these genes have sequence homology to the *mukBEF* genes from *E. coli*. These genes are involved in chromosome condensation and organization (52, 53). In *M. smegmatis* the genes MSMEG_1279–1281 are the result of a duplication of another region (MSMEG_0368–0370), which also share homology with the *mukBEF* genes. MSMEG_1282 contains a topoisomerase domain and is probably also involved in DNA organization.

If the genes MSMEG_1277–1282 do form a large operon, then the up-regulation seen in the microarray and qPCR may be due to loss of the autoregulation of this operon by Phd/Doc. If this was the case, then the up-regulation would also be seen in the Δ*phd/doc* but not in the other TA deletion strains. To test this hypothesis, qPCR investigating MSMEG_1279, MSMEG_1280, MSMEG_1281, and MSMEG_1282 expression levels in the wild type, Δ*mazEF* (RF100), Δ*phd/doc* (RF101), Δ*vapBC* (JR121), and the ΔTA^{triple} (RF105) was performed (Fig. 8*d*). The fold changes in the TA deletion strains were determined based on the values for the wild type. The four genes were all up-regulated in Δ*phd/doc* (RF101) and in ΔTA^{triple} mutant (Fig. 8*d*), confirming that it is due to deletion of the *phd/doc* genes or due to the introduction of the kanamycin resistance cassette used for creating the deletion. The Δ*phd/doc* strain RF101 does not have the same survival defect as ΔTA^{triple} (RF105) when grown for a long period of time in LBT (see supplemental Fig. S1). Based on this observation, we conclude that the up-regulation of these genes in the ΔTA^{triple} mutant are not likely to be the cause of the survival defect. Two of the genes were significantly down-regulated in the Δ*mazEF* strain; however, the change in expression was less than 2-fold. MSMEG_1282 was up-regulated in Δ*vapBC* 3-fold, but the reason for this is unknown. MSMEG_1282 has been shown to be part of a separate mRNA transcript to the *vapBC* TA system (22). However, the *vapBC* operon is autoregulated, and the promoter region overlaps with MSMEG_1282, so in the deletion strain the removal of the VapBC complex from binding to that region of the DNA may allow some up-regulation.

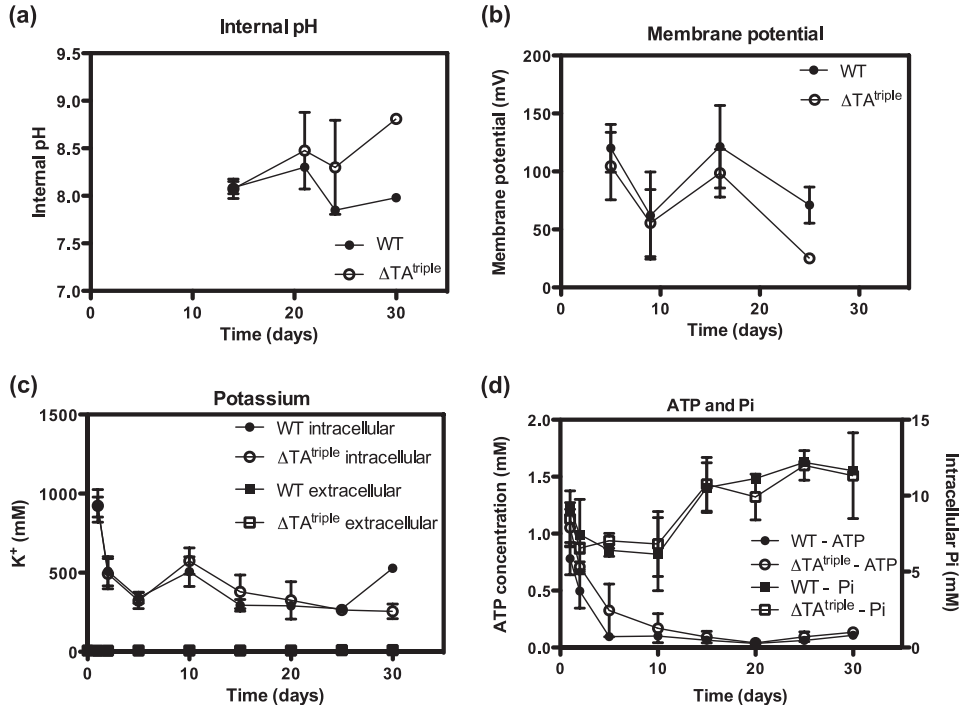

FIGURE 7. **Measurement of cellular parameters during long term survival in LBT.** *a,* internal pH of the cells was measured by uptake of [^{14}C]methylamine. *b,* membrane potential (mV) was measured by uptake of [^{3}H]TPP^{+}. *c,* intracellular and extracellular concentrations of K^{+} ions were determined by flame photometry. *d,* intracellular ATP and inorganic phosphate were measured as described under "Experimental Procedures." All data are shown as the mean ± S.D. for three biological replicates.

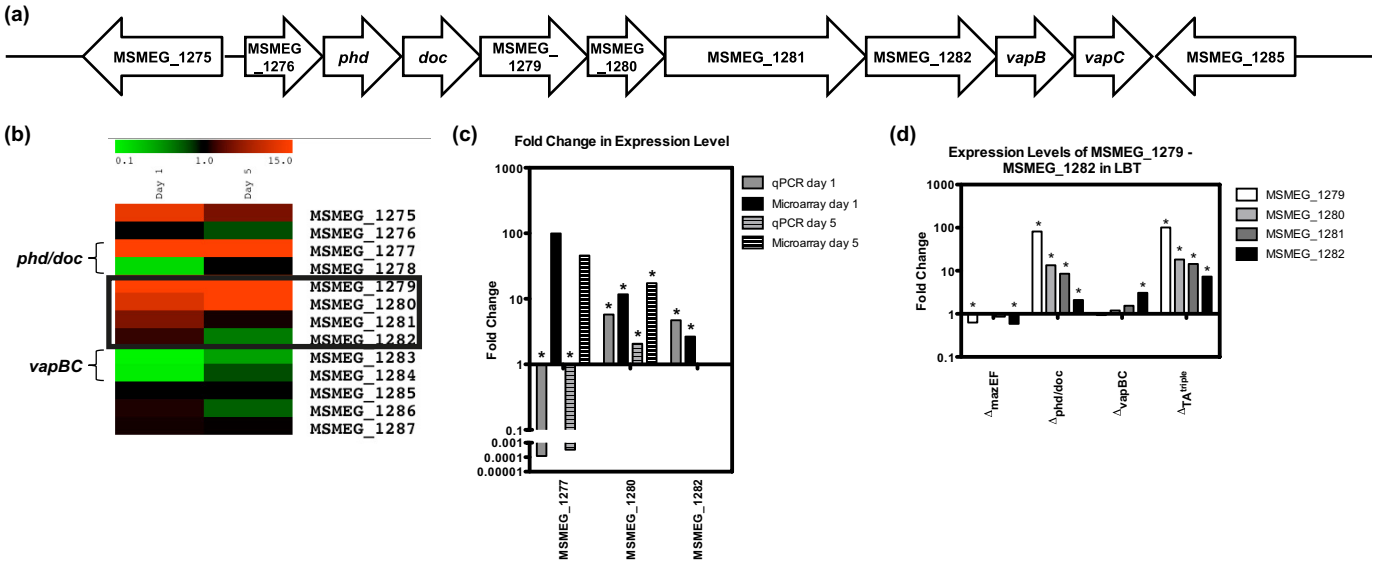

FIGURE 8. **Expression levels of MSMEG_1279-MSMEG_1282 in LBT.** *a,* schematic diagram of the TA systems *phd/doc* and *vapBC* and their surrounding genes. *b,* heat map generated by MIDAS showing the fold changes in expression levels of the *phd/doc* and *vapBC* TA systems and their surrounding genes from microarray analysis performed on wild type and Δ*mazEF*Δ*vapBC*Δ*phd/doc* (RF105) cultures grown in LBT for 1 day. The genes of interest (MSMEG_1279-MSMEG_1282) are *boxed*. *c,* fold changes in gene expression levels (Δ*mazEF*Δ*vapBC*Δ*phd/doc* (RF105)/wild type) for MSMEG_1277, MSMEG_1280, and MSMEG_1282 as determined by microarray analysis (*black bars*) and qPCR (*gray bars*) performed on the same RNA samples. Fold changes were tested for significance (*, $p \leq 0.005$). Results are shown as mean ± S.D. for four (*black bars*) and three (*gray bars*) biological replicates. *d,* fold changes in expression of the genes MSMEG_1279-MSMEG_1282 in Δ*mazEF* (RF100), Δ*phd/doc* (RF101), Δ*vapBC* (JR121), and Δ*mazEF*Δ*vapBC*Δ*phd/doc* (RF105) compared with wild type grown in LBT for 1 day. Fold changes were tested for significance (*, $p \leq 0.05$). Results are shown as mean ± S.D. for three biological replicates.

Metabolomic Analysis of Wild type and ΔTA^{triple} Mutant Cultures Reveals Differences in Intracellular Levels of Branched-chain Amino Acids—Because of the lack of significant differences in gene expression between the ΔTA^{triple} mutant and wild type, we propose the observed phenotype (survival defect) could be due to metabolic differences between the two strains. To address this hypothesis, we measured the extracellular and intracellular metabolite profile of the ΔTA^{triple} mutant and wild type grown in LBT for 15 days. The analysis identified 59 metabolites in the wild-type extracellular samples, 55 in RF105 extracellular samples, 57 in the wild-type intracellular samples, and 57 in RF105 intracellular samples from the in-house library

of MS spectra of ultra-pure metabolite standards (45). The metabolites that showed statistically significant differences (p value ≤ 0.05) between the wild type and ΔTA^{triple} mutant are shown in Fig. 9. At an extracellular level, the amino acids proline, lysine, phenylalanine, asparagine, threonine, glycine, aspartic acid, alanine, and glutamic acid were all depleted from the medium by both the wild type and ΔTA^{triple} mutant (Fig. 9*a*). Amino acid metabolism was in general higher in the ΔTA^{triple} mutant, particularly for lysine, proline, alanine, aspartate, and tryptophan (Fig. 9*a*). The majority of intracellular metabolites were similar between the wild type and ΔTA^{triple} mutant, but significant differences were observed for proline and the branched-chain amino acids leucine, isoleucine, and norleucine (Fig. 9*b*). Isoleucine was not detected in the ΔTA^{triple} mutant, but high levels of norleucine were present in the mutant and absent from the wild type. To address the hypothesis that a defect in the synthesis of the branched-chain amino acids leucine, isoleucine, and norleucine caused a survival defect in the ΔTA^{triple} mutant, we repeated the survival experiment in complex LBT medium containing the addition of leucine, isoleucine, and norleucine (all at 5 mM final concentration). As was observed in Fig. 6*c*, the ΔTA^{triple} mutant failed to survive past 15 days of starvation demonstrating that the mutant could not be rescued by exogenous branched-chain amino acids (data not shown).

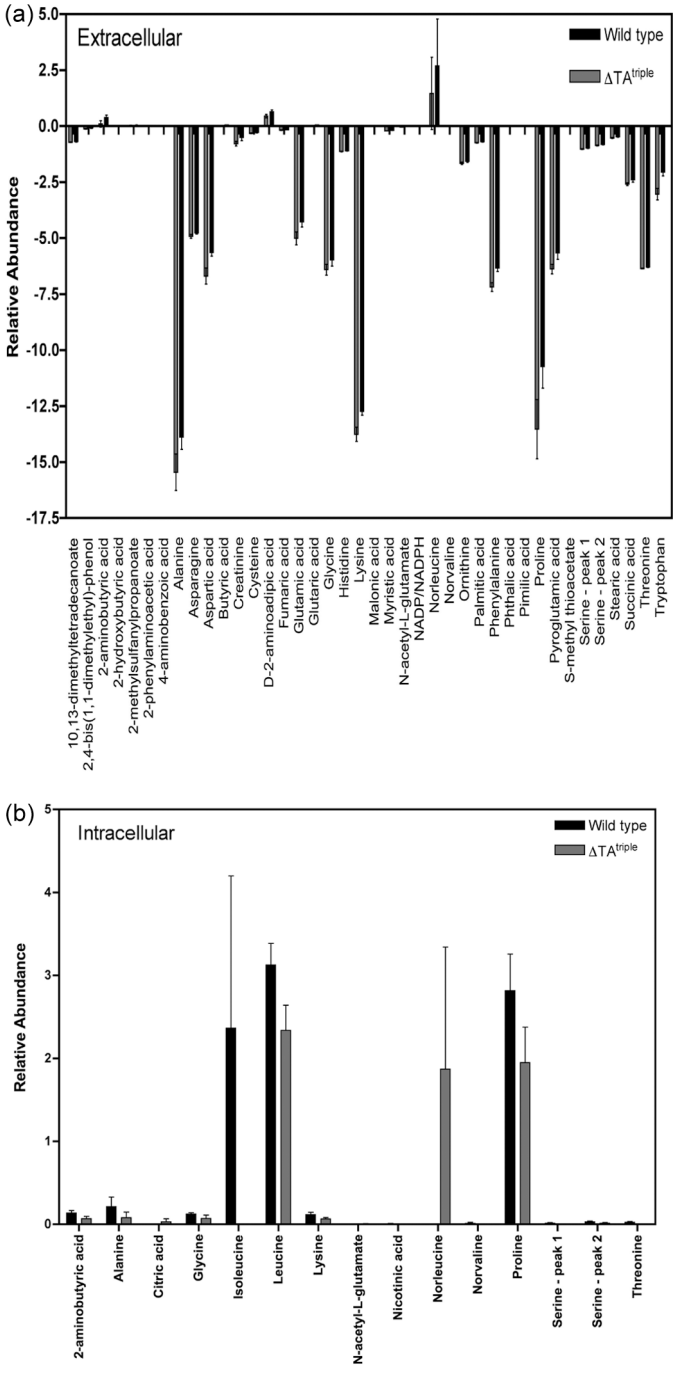

FIGURE 9. **Metabolite differences of *M. smegmatis* mc²155 wild type and ΔTA^{triple} after 15 days of growth in LBT.** Metabolites were extracted from cultures and analyzed by GC-MS, and the metabolic profiles were compared. The final relative concentration of metabolites was determined using the GC-peak intensity of methyl chloroformate derivatives. Compounds considered false-positives were then eliminated, and the intensity of each metabolite was normalized by the peak height of the internal standard (L-alanine-d_4). Because the amount of biomass was identical between replicates, no normalization by biomass was performed. The metabolites identified as statistically different between the strains as determined by analysis of variance ($p < 0.05$) for extracellular (*a*) and intracellular (*b*) samples are shown. Metabolites that were only identified in less than half the samples were considered false-positives and were not included. Results are from two biological replicates and three technical replicates from each strain. The error associated with these technical replicates is shown.

DISCUSSION

The genome of the bacterial pathogen *M. tuberculosis* harbors 88 putative TA systems (19, 21), and it has been hypothesized that these TA systems might be important during adaptation to changing growth rate, long term dormancy, and in generating bacilli that survive multidrug chemotherapy (54–56). Although this is an attractive hypothesis to explain the large number of TA systems present in *M. tuberculosis*, no studies have assessed overall TA function directly through gene deletion studies due to the extraordinary large number of genes involved. *M. smegmatis* contains only three TA systems (19, 22) and therefore represents an attractive model to uncover the role(s) of TA systems in a mycobacterial species.

In this study, we confirm that the open reading frames MSMEG_4447-MSMEG_4448 (*mazE-mazF*) and MSMEG_1277-MSMEG_1278 (*phd-doc*) encode *bona fide* TA modules, and in addition to the *vapBC* genes previously characterized (22), we demonstrate the presence of three functional TA modules in *M. smegmatis*. All three TA modules were expressed as leaderless transcripts throughout the growth cycle and autoregulated by the TA complex. Leaderless transcripts are translated more efficiently during adverse conditions such as carbon limitation, stationary phase, and slow growth, due to a higher prevalence of 70 S monosomes (57–59), and this feature would be congruent with the role of TA systems in responding to cell stress (5, 60). Many studies have sought to define a role for TA systems through overexpression of TA systems in the native host and in non-native hosts (*i.e.* typically *E. coli*). For example, the genome of *M. tuberculosis* harbors 47 homologs of the VapC family, 9 of MazF, 3 of RelE, 2 of ParD, 1 of HigB, and 26 novel systems (21). Of the 88 putative TA systems identified, 78 were cloned and expressed in *M. smegmatis*, and 30 were confirmed to function as TA systems (21). In a separate study, 30 out of 38 putative TA systems from *M. tuberculosis* were functional when expressed in *E. coli* (61). Of the nine MazF

homologs identified in *M. tuberculosis*, seven have been studied and shown to cause growth arrest when expressed in *E. coli* (49, 62, 63). Han *et al.* (55) reported that expression of Rc1102c in *M. smegmatis*, a mRNA interferase (49), caused a reversible bacteriostasis and contributed to the formation of drug-tolerant persisters in *M. smegmatis*. Survival of the ΔTA^{triple} *M. smegmatis* mutant to streptomycin and rifampin challenge was not impaired compared with the wild-type cells suggesting that the three TA modules in *M. smegmatis* were not required to generate drug-tolerant cells. *M. tuberculosis* harbors three Rel toxin-antitoxin module, and expression of all three in *M. smegmatis* and *M. tuberculosis* caused growth inhibition that was neutralized by their respective cognate antitoxin (64, 65). Further worked showed that expression of the RelE2 toxin in *M. tuberculosis* induced the formation of drug-specific persisters *in vitro*; however, deletion of *relE2* did not affect the level of persisters of *M. tuberculosis* in rifampin-treated mice ruling out a role for *relE2* in the generation of bacilli that survive multidrug therapy (66). The *M. smegmatis* genome contains no *rel* homologs but does contain a *phd/doc* module not found in *M. tuberculosis*. Based on these studies, mycobacteria harbor a number of TA modules that can contribute to growth arrest and persistence to drugs. However, it is important to note that in none of the aforementioned studies was the TA module-mediated cell bacteriostasis/inhibition shown to function in a physiologically relevant situation, and therefore, more studies are required in this area to ascertain the biological role(s) of TA systems in *M. tuberculosis*.

To gain a better understanding of the role of TA systems in a native host, a strain of *E. coli* was created in which all TA systems were deleted, *i.e.* Δ*mazEF* Δ*relBE* Δ*chpB* Δ*yefM-yoeB* Δ*dinJ-yafQ* (designated Δ5) (16). The Δ5 mutant was studied to determine its ability to survive and recover from various stresses compared with the isogenic wild type. All of these *E. coli* toxins cause mRNA cleavage and have been proposed to be involved in responding to stress (7, 8, 67–70). Surprisingly, given the previous literature on these TA systems in *E. coli*, there was no significant difference between the Δ5 mutant and wild type when challenged with rifampicin, amino acid starvation, acidic stress, or nutritional downshift (16). Additionally there was no difference in competition experiments during amino acid starvation, nutritional downshift, or long term cultures. This study was not able to find a benefit or a disadvantage to having these five TA systems in the chromosome of *E. coli*. Only recently did researchers show that the Δ5 strain was found to form less biofilm after 8 h and more biofilm after 24 h (17). Transcriptome analysis identified only one gene (*yjgK*) that was differentially regulated in the Δ5 compared with the wild type under these conditions (17). The product of this gene, YjgK, was found to repress fimbriae, which are needed for formation of the biofilm, but are not required when cells are released from the biofilm into planktonic growth. Similar studies have been performed in *Streptococcus mutans*, which harbors two TA systems in its genome, one from the *mazEF* family and one from the *relBE* family (71).

To provide a molecular model for the role of TA systems in mycobacteria, we deleted all three TA modules in *M. smegmatis*. A number of typical stressors were tested (*e.g.* antibiotic stress, mitomycin C, nalidixic acid, acid pH, iron chelators, high pH, heat shock, and oxidative stress), and only for oxidative and heat shock stress did we observe a difference between the wild type and the mutant, and in both cases the mutant was more susceptible than the wild type to the imposed stress. When the ΔTA^{triple} mutant was grown in complex medium and viability was monitored over an extended period, a survival defect was observed. Cell death was not due to a critical ion (K^+) or intracellular ATP loss, and the membrane potential and internal pH of the ΔTA^{triple} mutant was comparable with the wild-type strain. The survival defect of the ΔTA^{triple} mutant was not observed in either minimal medium or PBS-T aerobically or in LBT medium under anaerobic conditions, but it was unique to complex medium. We hypothesize that this survival defect is due to the combination of stressors that mycobacterial cells encounter in complex medium after aerobic growth, *i.e.* high cell density, high pH, accumulation of reactive oxygen species, and toxic end products. Consistent with this hypothesis was the observation that we could not rescue the survival defect of the ΔTA^{triple} mutant with single nutrients (*e.g.* excess iron, carbon, nitrogen, or phosphate) and were unable to isolate suppressor mutants to this phenotype, which suggested a complex network of cellular changes. No significant differences at a transcriptional level were noted between the wild type and ΔTA^{triple} mutant, which is similar to findings reported for studies performed with the *E. coli* Δ5 mutant *versus* wild type (16).

Analysis of the intracellular and extracellular metabolites of the wild type and ΔTA^{triple} mutant at day 15 in LBT medium revealed that the catabolism of *M. smegmatis* was geared toward the metabolism of amino acids. Analysis of the intracellular metabolite profile revealed significant variations in the intracellular levels of the branched-chain amino acids leucine and isoleucine. The intracellular concentration of branched-chain amino acids in bacteria has been linked to the nutritional supply and physiological state of the cell (72, 73), as well as serving a central role in linking catabolism with anabolism (74). Isoleucine was not detected in the ΔTA^{triple} mutant, and high levels of norleucine were detected. Norleucine is a methionine analog that is incorporated into proteins in place of methionine. We propose that due to the high levels of intracellular norleucine in the ΔTA^{triple} mutant, it is highly likely that norleucine is incorporated into proteins under these conditions. Methionine has been shown to act as an endogenous antioxidant protecting the protein in which they are located and other macromolecules (75). In contrast, proteins with norleucine incorporated have been shown to be more sensitive to oxidative damage (75). Moreover, oxidatively damaged *Salmonella typhimurium* can be rescued by the addition of branched-chain amino acids (76) suggesting a potential link between branched-chain amino acids and oxidative stress in bacteria. The ΔTA^{triple} mutant was more sensitive to H_2O_2 stress compared with the wild type, and taken together these observations suggest a potential link between cell death (oxidative stress-mediated) of the mutant and accumulation of intracellular branched-chain amino acids. The role of TA modules in regulating nitrogen and carbon flux (*e.g.* amino acids) in mycobacteria remains to be investigated.

REFERENCES

1. Ogura, T., and Hiraga, S. (1983) Mini-F plasmid genes that couple host cell division to plasmid proliferation. *Proc. Natl. Acad. Sci. U.S.A.* **80,** 4784–4788
2. Jaffé, A., Ogura, T., and Hiraga, S. (1985) Effects of the ccd function of the F plasmid on bacterial growth. *J. Bacteriol.* **163,** 841–849
3. Magnuson, R. D. (2007) Hypothetical functions of toxin-antitoxin systems. *J. Bacteriol.* **189,** 6089–6092
4. Fineran, P. C., Blower, T. R., Foulds, I. J., Humphreys, D. P., Lilley, K. S., and Salmond, G. P. (2009) The phage abortive infection system, ToxIN, functions as a protein-RNA toxin-antitoxin pair. *Proc. Natl. Acad. Sci. U.S.A.* **106,** 894–899
5. Gerdes, K., Christensen, S. K., and Løbner-Olesen, A. (2005) Prokaryotic toxin-antitoxin stress-response loci. *Nat. Rev. Microbiol.* **3,** 371–382
6. Van Melderen, L., and Saavedra De Bast, M. (2009) Bacterial toxin-antitoxin systems. More than selfish entities? *PLoS Genet.* **5,** e1000437
7. Zhang, Y., Zhang, J., Hoeflich, K. P., Ikura, M., Qing, G., and Inouye, M. (2003) MazF cleaves cellular mRNAs specifically at ACA to block protein synthesis in *Escherichia coli*. *Mol. Cell* **12,** 913–923
8. Pedersen, K., Zavialov, A. V., Pavlov, M. Y., Elf, J., Gerdes, K., and Ehrenberg, M. (2003) The bacterial toxin RelE displays codon-specific cleavage of mRNAs in the ribosomal A site. *Cell* **112,** 131–140
9. Arcus, V. L., Bäckbro, K., Roos, A., Daniel, E. L., and Baker, E. N. (2004) Distant structural homology leads to the functional characterization of an archaeal PIN domain as an exonuclease. *J. Biol. Chem.* **279,** 16471–16478
10. Christensen-Dalsgaard, M., and Gerdes, K. (2006) Two higBA loci in the *Vibrio cholerae* superintegron encode mRNA cleaving enzymes and can stabilize plasmids. *Mol. Microbiol.* **62,** 397–411
11. Jiang, Y., Pogliano, J., Helinski, D. R., and Konieczny, I. (2002) ParE toxin encoded by the broad-host-range plasmid RK2 is an inhibitor of *Escherichia coli* gyrase. *Mol. Microbiol.* **44,** 971–979
12. Bernard, P., and Couturier, M. (1992) Cell killing by the F plasmid CcdB protein involves poisoning of DNA-topoisomerase II complexes. *J. Mol. Biol.* **226,** 735–745
13. Maki, S., Takiguchi, S., Miki, T., and Horiuchi, T. (1992) Modulation of DNA supercoiling activity of *Escherichia coli* DNA gyrase by F plasmid proteins. Antagonistic actions of LetA (CcdA) and LetD (CcdB) proteins. *J. Biol. Chem.* **267,** 12244–12251
14. Liu, M., Zhang, Y., Inouye, M., and Woychik, N. A. (2008) Bacterial addiction module toxin Doc inhibits translation elongation through its association with the 30 S ribosomal subunit. *Proc. Natl. Acad. Sci. U.S.A.* **105,** 5885–5890
15. Schumacher, M. A., Piro, K. M., Xu, W., Hansen, S., Lewis, K., and Brennan, R. G. (2009) Molecular mechanisms of HipA-mediated multidrug tolerance and its neutralization by HipB. *Science* **323,** 396–401
16. Tsilibaris, V., Maenhaut-Michel, G., Mine, N., and Van Melderen, L. (2007) What is the benefit to Escherichia coli of having multiple toxin-antitoxin systems in its genome? *J. Bacteriol.* **189,** 6101–6108
17. Kim, Y., Wang, X., Ma, Q., Zhang, X. S., and Wood, T. K. (2009) Toxin-antitoxin systems in *Escherichia coli* influence biofilm formation through YjgK (TabA) and fimbriae. *J. Bacteriol.* **191,** 1258–1267
18. Kolodkin-Gal, I., Verdiger, R., Shlosberg-Fedida, A., and Engelberg-Kulka, H. (2009) A differential effect of *E. coli* toxin-antitoxin systems on cell death in liquid media and biofilm formation. *PLoS One* **4,** e6785
19. Pandey, D. P., and Gerdes, K. (2005) Toxin-antitoxin loci are highly abundant in free-living but lost from host-associated prokaryotes. *Nucleic Acids Res.* **33,** 966–976
20. Anantharaman, V., and Aravind, L. (2003) New connections in the prokaryotic toxin-antitoxin network. Relationship with the eukaryotic nonsense-mediated RNA decay system. *Genome Biol.* **4,** R81
21. Ramage, H. R., Connolly, L. E., and Cox, J. S. (2009) Comprehensive functional analysis of *Mycobacterium tuberculosis* toxin-antitoxin systems. Implications for pathogenesis, stress responses, and evolution. *PLoS Genet.* **5,** e1000767
22. Robson, J., McKenzie, J. L., Cursons, R., Cook, G. M., and Arcus, V. L. (2009) The vapBC operon from *Mycobacterium smegmatis* is an autoregulated toxin-antitoxin module that controls growth via inhibition of translation. *J. Mol. Biol.* **390,** 353–367
23. Arcus, V. L., McKenzie, J. L., Robson, J., and Cook, G. M. (2011) The PIN-domain ribonucleases and the prokaryotic VapBC toxin-antitoxin array. *Protein Eng. Des. Sel.* **24,** 33–40
24. Hopper, S., Wilbur, J. S., Vasquez, B. L., Larson, J., Clary, S., Mehr, I. J., Seifert, H. S., and So, M. (2000) Isolation of *Neisseria gonorrhoeae* mutants that show enhanced trafficking across polarized T84 epithelial monolayers. *Infect. Immun.* **68,** 896–905
25. Smeulders, M. J., Keer, J., Speight, R. A., and Williams, H. D. (1999) Adaptation of *Mycobacterium smegmatis* to stationary phase. *J. Bacteriol.* **181,** 270–283
26. Bull, T. J., Hermon-Taylor, J., Pavlik, I., El-Zaatari, F., and Tizard, M. (2000) Characterization of IS900 loci in *Mycobacterium avium* subsp. *paratuberculosis* and development of multiplex PCR typing. *Microbiology* **146,** 2185–2197
27. Guo, X. V., Monteleone, M., Klotzsche, M., Kamionka, A., Hillen, W., Braunstein, M., Ehrt, S., and Schnappinger, D. (2007) Silencing *Mycobacterium smegmatis* by using tetracycline repressors. *J. Bacteriol.* **189,** 4614–4623
28. Ehrt, S., Guo, X. V., Hickey, C. M., Ryou, M., Monteleone, M., Riley, L. W., and Schnappinger, D. (2005) Controlling gene expression in mycobacteria with anhydrotetracycline and Tet repressor. *Nucleic Acids Res.* **33,** e21
29. Blokpoel, M. C., Murphy, H. N., O'Toole, R., Wiles, S., Runn, E. S., Stewart, G. R., Young, D. B., and Robertson, B. D. (2005) Tetracycline-inducible gene regulation in mycobacteria. *Nucleic Acids Res.* **33,** e22
30. Gebhard, S., Tran, S. L., and Cook, G. M. (2006) The Phn system of *Mycobacterium smegmatis*. A second high-affinity ABC transporter for phosphate. *Microbiology* **152,** 3453–3465
31. Pelicic, V., Reyrat, J. M., and Gicquel, B. (1996) Generation of unmarked directed mutations in mycobacteria, using sucrose counter-selectable suicide vectors. *Mol. Microbiol.* **20,** 919–925
32. Pelicic, V., Jackson, M., Reyrat, J. M., Jacobs, W. R., Jr., Gicquel, B., and Guilhot, C. (1997) Efficient allelic exchange and transposon mutagenesis in *Mycobacterium tuberculosis*. *Proc. Natl. Acad. Sci. U.S.A.* **94,** 10955–10960
33. Ménard, R., Sansonetti, P. J., and Parsot, C. (1993) Nonpolar mutagenesis of the *ipa* genes defines IpaB, IpaC, and IpaD as effectors of *Shigella flexneri* entry into epithelial cells. *J. Bacteriol.* **175,** 5899–5906
34. Timm, J., Lim, E. M., and Gicquel, B. (1994) *Escherichia coli*-mycobacteria shuttle vectors for operon and gene fusions to *lacZ*. The pJEM series. *J. Bacteriol.* **176,** 6749–6753
35. Dussurget, O., Timm, J., Gomez, M., Gold, B., Yu, S., Sabol, S. Z., Holmes, R. K., Jacobs, W. R., Jr., and Smith, I. (1999) Transcriptional control of the iron-responsive *fxbA* gene by the mycobacterial regulator IdeR. *J. Bacteriol.* **181,** 3402–3408
36. Rao, M., Streur, T. L., Aldwell, F. E., and Cook, G. M. (2001) Intracellular pH regulation by *Mycobacterium smegmatis* and *Mycobacterium bovis* BCG. *Microbiology* **147,** 1017–1024
37. Zilberstein, D., Agmon, V., Schuldiner, S., and Padan, E. (1982) The sodium/proton antiporter is part of the pH homeostasis mechanism in *Escherichia coli*. *J. Biol. Chem.* **257,** 3687–3691
38. Horn, D. B., and Squire, C. R. (1966) The estimation of ammonia using the indophenol blue reaction. *Clin. Chim. Acta* **14,** 185–194
39. Mantovani, H. C., Hu, H., Worobo, R. W., and Russell, J. B. (2002) Bovicin HC5, a bacteriocin from *Streptococcus bovis* HC5. *Microbiology* **148,** 3347–3352
40. Larsson, C. M., and Olsson, T. (1979) Firefly assay of adenine nucleotides from algae. Comparison of extraction methods. *Plant Cell Physiol.* **20,** 145–155
41. Lundin, A., and Thore, A. (1975) Analytical information obtainable by evaluation of the time course of firefly bioluminescence in the assay of ATP. *Anal. Biochem.* **66,** 47–63
42. Monk, B. C., Kurtz, M. B., Marrinan, J. A., and Perlin, D. S. (1991) Cloning and characterization of the plasma membrane H(+)-ATPase from *Candida albicans*. *J. Bacteriol.* **173,** 6826–6836
43. Villas-Bôas, S. G., and Bruheim, P. (2007) Cold glycerol-saline. The promising quenching solution for accurate intracellular metabolite analysis of microbial cells. *Anal. Biochem.* **370,** 87–97

44. Berney, M., and Cook, G. M. (2010) Unique flexibility in energy metabolism allows mycobacteria to combat starvation and hypoxia. *PloS One* **5,** e8614
45. Smart, K. F., Aggio, R. B., Van Houtte, J. R., and Villas-Bôas, S. G. (2010) Analytical platform for metabolome analysis of microbial cells using MCF derivatization followed by gas chromatography-mass spectrometry. *Nat. Protoc.* **5,** 1709–1729
46. Aggio, R. B., Ruggiero, K., and Villas-Bôas, S. G. (2010) Pathway Activity Profiling (PAPi). From the metabolite profile to the metabolic pathway activity. *Bioinformatics* **26,** 2969–2976
47. Aizenman, E., Engelberg-Kulka, H., and Glaser, G. (1996) An *Escherichia coli* chromosomal "addiction module" regulated by guanosine (corrected) 3′,5′-bispyrophosphate. A model for programmed bacterial cell death. *Proc. Natl. Acad. Sci. U.S.A.* **93,** 6059–6063
48. Pellegrini, O., Mathy, N., Gogos, A., Shapiro, L., and Condon, C. (2005) The *Bacillus subtilis* ydcDE operon encodes an endoribonuclease of the MazF/PemK family and its inhibitor. *Mol. Microbiol.* **56,** 1139–1148
49. Zhu, L., Zhang, Y., Teh, J. S., Zhang, J., Connell, N., Rubin, H., and Inouye, M. (2006) Characterization of mRNA interferases from *Mycobacterium tuberculosis*. *J. Biol. Chem.* **281,** 18638–18643
50. Fu, Z., Donegan, N. P., Memmi, G., and Cheung, A. L. (2007) Characterization of MazFSa, an endoribonuclease from *Staphylococcus aureus*. *J. Bacteriol.* **189,** 8871–8879
51. Syed, M. A., Koyanagi, S., Sharma, E., Jobin, M. C., Yakunin, A. F., and Lévesque, C. M. (2011) The chromosomal mazEF locus of *Streptococcus mutans* encodes a functional type II toxin-antitoxin addiction system. *J. Bacteriol.* **193,** 1122–1130
52. Hiraga, S., Niki, H., Ogura, T., Ichinose, C., Mori, H., Ezaki, B., and Jaffé, A. (1989) Chromosome partitioning in *Escherichia coli*. Novel mutants producing anucleate cells. *J. Bacteriol.* **171,** 1496–1505
53. Yamanaka, K., Ogura, T., Niki, H., and Hiraga, S. (1996) Identification of two new genes, *mukE* and *mukF*, involved in chromosome partitioning in *Escherichia coli*. *Mol. Gen. Genet.* **250,** 241–251
54. Dahl, J. L., Kraus, C. N., Boshoff, H. I., Doan, B., Foley, K., Avarbock, D., Kaplan, G., Mizrahi, V., Rubin, H., and Barry, C. E., 3rd (2003) The role of RelMtb-mediated adaptation to stationary phase in long term persistence of *Mycobacterium tuberculosis* in mice. *Proc. Natl. Acad. Sci. U.S.A.* **100,** 10026–10031
55. Han, J. S., Lee, J. J., Anandan, T., Zeng, M., Sripathi, S., Jahng, W. J., Lee, S. H., Suh, J. W., and Kang, C. M. (2010) Characterization of a chromosomal toxin-antitoxin, Rv1102c-Rv1103c system in *Mycobacterium tuberculosis*. *Biochem. Biophys. Res. Commun.* **400,** 293–298
56. Beste, D. J., Espasa, M., Bonde, B., Kierzek, A. M., Stewart, G. R., and McFadden, J. (2009) The genetic requirements for fast and slow growth in mycobacteria. *PLoS One* **4,** e5349
57. Uchida, T., Abe, M., Matsuo, K., and Yoneda, M. (1970) Amounts of free 70 S ribosomes and ribosomal subunits found in *Escherichia coli* at various temperatures. *Biochem. Biophys. Res. Commun.* **41,** 1048–1054
58. Ruscetti, F. W., and Jacobson, L. A. (1972) Accumulation of 70 S monoribosomes in *Escherichia coli* after energy source shift-down. *J. Bacteriol.* **111,** 142–151
59. Moll, I., Hirokawa, G., Kiel, M. C., Kaji, A., and Bläsi, U. (2004) Translation initiation with 70 S ribosomes. An alternative pathway for leaderless mRNAs. *Nucleic Acids Res.* **32,** 3354–3363
60. Buts, L., Lah, J., Dao-Thi, M. H., Wyns, L., and Loris, R. (2005) Toxin-antitoxin modules as bacterial metabolic stress managers. *Trends Biochem. Sci.* **30,** 672–679
61. Gupta, A. (2009) Killing activity and rescue function of genome-wide toxin-antitoxin loci of *Mycobacterium tuberculosis*. *FEMS Microbiol. Lett.* **290,** 45–53
62. Zhu, L., Phadtare, S., Nariya, H., Ouyang, M., Husson, R. N., and Inouye, M. (2008) The mRNA interferases, MazF-mt3 and MazF-mt7, from *Mycobacterium tuberculosis* target unique pentad sequences in single-stranded RNA. *Mol. Microbiol.* **69,** 559–569
63. Zhao, L., and Zhang, J. (2008) Biochemical characterization of a chromosomal toxin-antitoxin system in *Mycobacterium tuberculosis*. *FEBS Lett.* **582,** 710–714
64. Korch, S. B., Contreras, H., and Clark-Curtiss, J. E. (2009) Three *Mycobacterium tuberculosis* Rel toxin-antitoxin modules inhibit mycobacterial growth and are expressed in infected human macrophages. *J. Bacteriol.* **191,** 1618–1630
65. Yang, M., Gao, C., Wang, Y., Zhang, H., and He, Z. G. (2010) Characterization of the interaction and cross-regulation of three *Mycobacterium tuberculosis* RelBE modules. *PLoS One* **5,** e10672
66. Singh, R., Barry, C. E., 3rd, and Boshoff, H. I. (2010) The three RelE homologs of *Mycobacterium tuberculosis* have individual, drug-specific effects on bacterial antibiotic tolerance. *J. Bacteriol.* **192,** 1279–1291
67. Zhang, Y., Yamaguchi, Y., and Inouye, M. (2009) Characterization of YafO, an *Escherichia coli* toxin. *J. Biol. Chem.* **284,** 25522–25531
68. Christensen, S. K., and Gerdes, K. (2004) Delayed-relaxed response explained by hyperactivation of RelE. *Mol. Microbiol.* **53,** 587–597
69. Christensen-Dalsgaard, M., and Gerdes, K. (2008) Translation affects YoeB and MazF messenger RNA interferase activities by different mechanisms. *Nucleic Acids Res.* **36,** 6472–6481
70. Zhang, Y., Zhu, L., Zhang, J., and Inouye, M. (2005) Characterization of ChpBK, an mRNA interferase from *Escherichia coli*. *J. Biol. Chem.* **280,** 26080–26088
71. Lemos, J. A., Brown, T. A., Jr., Abranches, J., and Burne, R. A. (2005) Characteristics of *Streptococcus mutans* strains lacking the MazEF and RelBE toxin-antitoxin modules. *FEMS Microbiol. Lett.* **253,** 251–257
72. Shivers, R. P., and Sonenshein, A. L. (2004) Activation of the *Bacillus subtilis* global regulator CodY by direct interaction with branched-chain amino acids. *Mol. Microbiol.* **53,** 599–611
73. Guédon, E., Serror, P., Ehrlich, S. D., Renault, P., and Delorme, C. (2001) Pleiotropic transcriptional repressor CodY senses the intracellular pool of branched-chain amino acids in *Lactococcus lactis*. *Mol. Microbiol.* **40,** 1227–1239
74. Tojo, S., Satomura, T., Morisaki, K., Deutscher, J., Hirooka, K., and Fujita, Y. (2005) Elaborate transcription regulation of the *Bacillus subtilis ilv-leu* operon involved in the biosynthesis of branched-chain amino acids through global regulators of CcpA, CodY, and TnrA. *Mol. Microbiol.* **56,** 1560–1573
75. Luo, S., and Levine, R. L. (2009) Methionine in proteins defends against oxidative stress. *FASEB J.* **23,** 464–472
76. Blum, P. H. (1988) Reduced leu operon expression in a miaA mutant of *Salmonella typhimurium*. *J. Bacteriol.* **170,** 5125–5133
77. Hanahan, D., Jessee, J., and Bloom, F. R. (1991) Plasmid transformation of *Escherichia coli* and other bacteria. *Methods Enzymol.* **204,** 63–113
78. Snapper, S. B., Melton, R. E., Mustafa, S., Kieser, T., and Jacobs, W. R., Jr. (1990) Isolation and characterization of efficient plasmid transformation mutants of *Mycobacterium smegmatis*. *Mol. Microbiol.* **4,** 1911–1919